Hallmarks of Reversible Phase Separation in Living, Unperturbed Cell Membranes

Scott P. Rayermann

A dissertation
submitted in partial fulfillment of the
requirements for the degree of

Doctor of Philosophy

University of Washington
2017

Reading Committee:
Sarah L. Keller, Chair
Cody W. Schlenker
Joshua C. Vaughan

Program Authorized to Offer Degree:
Chemistry

University of Washington

Abstract

Hallmarks of Reversible Phase Separation in Living, Unperturbed Cell Membranes

Scott P. Rayermann

Chair of Supervisory Committee:
Professor Sarah L. Keller
Department of Chemistry

Controversy has long surrounded the question of whether spontaneous lateral demixing of membranes into coexisting liquid phases can organize proteins and lipids on micron scales within unperturbed, living cells. A clear answer hinges on observation of hallmarks of a reversible phase transition. Here, by directly imaging micron-scale membrane domains of yeast vacuoles both in vivo and cell-free, we demonstrate that the domains arise through a phase separation mechanism. The domains are large, have smooth boundaries, and can merge quickly, consistent with fluid phases. Moreover, the domains disappear above a distinct miscibility transition temperature (Tmix) and reappear below Tmix, over multiple heating and cooling cycles. Hence, large-scale membrane organization in living cells under physiologically relevant conditions can be controlled by tuning a single thermodynamic parameter.

Dedication

To science!

Acknowledgements

I have had the privilege of receiving mentorship, training, and encouragement from a vast array of individuals while working on my Ph.D. I value all of them for supporting my efforts to earn a higher degree. I would like to take this opportunity to directly thank them here.

I have collaborated with many scientists who provided me with invaluable insights, expertise, and training. My own success is thanks in large part to their efforts and I would like to acknowledge specifically my advisers and mentors Prof. Sarah L. Keller and Prof. Alex J. Merz. In addition to their own mentorship, I consulted members of both their labs for advice and insights into my experiments. I would like to thank all the members of the Keller and Merz labs for sharing their experience and expertise with me.

I also want to thank the University of Washington's staff. It is largely due to their efforts that I was able to focus on my research. I would like to give particular thanks to the Chemistry Department's Front Office staff, the Chemistry Department's lab techs, and the University's building and maintenance staff. Thanks to their support in maintaining documentation and answering questions on requirements, streamlining my responsibilities as a teaching assistant, and keeping my workspaces clean and functional, I was able to progress on my degree quickly and efficiently.

My friends and family provided me with constant support. They put up with both my complaints and my inarticulate glee over experimental progress. Further, they offered emotional support and advice as I worked out coping mechanisms for seasonal affective disorder. There is no doubt in my mind that I relied on the strength of my personal relationships and I cannot thank my friends and family enough for their love.

Finally, I would like to thank you, the reader. Scientist seek to expand humanity's knowledge and I am proud to contribute to this noble endeavor. I write this document in the hope that it will preserve the knowledge I worked so hard to discover. To be truly useful, however, this knowledge must be shared, so thank you, dear reader, for helping to keep the knowledge in this document alive. I hope you find something of use to you in these pages.

Nomenclature

GPMV	Giant Plasma Membrane Vesicle – a vesicle derived from the plasma membrane of a cell by inducing blebbing and shaking the system to separate the bleb from the parent plasma membrane
GUV	Giant Unilamellar Vesicle – a purely synthetic vesicle on the order of 100 microns in diameter created by mixing lipids in a desired ratio
HILO	Highly Inclined and Laminated Optical sheet
RBL	Rat Basophilic Leukemia
SC	Synthetic Complete media; a yeast growth medium with the amino acid, sulfate, and D-glucose needed to mimic the auxotrophic support provided by YPD media without the variable, extra components in yeast extract.
YPD	Yeast extract peptone dextrose; a rich yeast growth medium composed of yeast extracts, peptone, and D-glucose that provides all yeast amino acids, allowing any auxotroph to grow in it.

Table of Contents

List of Figures and Tables

CHAPTER 0

Note on Collaborative Research

Science is a collaborative endeavor and I enjoyed working with many talented scientists throughout my dissertation. These collaborations resulted in two manuscripts for publication. Significant sections of this dissertation are reproduced verbatim from these multi-author works. Ahead of these sections, a notice is given to the reader to provide full references and acknowledge all authors. Each university differs in its requirements for how to acknowledge collaborations in Ph.D. dissertations. The University of Washington does not require attribution of individual figures, data sets, or sections of text to specific authors. I would like to acknowledge at the beginning of my dissertation that all the authors provided important and valuable contributions to each manuscript, and in turn to the content of this dissertation. Those authors are Dr. Matthew C. Blosser, Caitlin E. Cornell, Glennis E. Rayermann, Scott P. Rayermann, Prof. Alex J. Merz, and Prof. Sarah L. Keller. To increase the readability of the dissertation, I have kept individual attributions within the main text to a minimum.

CHAPTER 1

Introduction

1.1 General Overview

This general overview is taken from section Chapter 4, section 2 (4.2) below.

Scientists have invested decades of effort in probing the lipid and protein composition of cell membranes for evidence of heterogeneity, which has the potential to control protein sorting, signal transduction, and other processes.[1] Aside from a few important exceptions, that extensive body of work has implied that the length scale of compositional heterogeneity in the membranes of unstimulated cells is limited to nanoscales.[2] Sub-micron domains in membranes gained notoriety as "rafts," and, more recently, as dynamic, short-lived "platforms."[2,3] These concepts are controversial because both terms are loosely and sometimes inconsistently defined, and because nanoscale domains are, at best, challenging to observe directly. In contrast, model lipid membranes spontaneously demix on large (μm) length scales, into two well-defined liquid phases. This demixing follows clear thermodynamic principles.[4,5] The concept of phase separation is subject to established, quantitative rules that enable rigorous verification of predictions. These rules apply equally well to simple bilayer membranes composed of only three types of lipids, to the complex bilayer membranes of giant plasma membrane vesicles blebbed from cells, and to phase-separated cytoplasmic droplets recently implicated across a variety of cell biological activities.[6–8]

1.2 Phase Separation in Giant Unilamellar Vesicles

Giant Unilamellar Vesicles (GUVs) are spherical membrane structures on the order of 100 microns in diameter and composed of a single lipid bilayer.[9] Some membranes composed of

at least three different types of lipids – one a sterol – can separate into two coexisting liquid phases.[4,10] Section 1.2 focuses on the phase behavior of these systems.

1.2.1 Source

The following are select passages from the chapter "Phase Diagrams and Tie Lines in GUVs," from *The Giant Vesicle Book*. Rumiana Dimova and Carlos M. Marques, eds. Boca Raton: Taylor & Francis / CRC Press (2018), which I co-authored with Matthew C. Blosser, Caitlin E. Cornell, and Sarah L. Keller.[11]

1.2.2 Introduction

In many types of GUVs composed of mixtures of lipids and sterols, a dramatic change occurs when the temperature of the system decreases: the membrane spontaneously demixes into two or more coexisting phases. This phenomenon has attracted the attention of researchers from a wide range of fields. From a biological perspective, the ease with which model lipid membranes phase separate into two liquid phases lends credence to proposals that lipids in cell membranes may be poised to demix.[12,13] Demixing of cell membranes is particularly relevant with respect to its possible effects on protein behavior. In model systems, proteins partition differently into the two membrane phases, and protein activities are affected by the local lipid composition of the membrane.[14–19] From a physical perspective, coexisting phases in lipid membranes provide an ideal quasi 2-dimensional system in which to test fundamental theories.

1.2.3 Identifying Coexisting Phases in GUVs

Microscopy of GUVs is one of several powerful tools for identifying lipid phase behavior. Inferring membrane phases from micron-scale observations requires familiarity with the characteristics of each phase.

1.2.3.1 An Intuitive Analogy About Demixing of Liquid Phases

To gain an intuition about the demixing of a membrane into two liquid phases and about tie lines, consider the following analogy. Imagine that you are suddenly transported into the middle of a crowded party in a large, open room where nobody previously knows each other. As people move, they jostle each other. As people laterally diffuse across the entire room, they talk with each other, which results in either favorable or unfavorable interactions. People involved in favorable interactions assemble into groups. Individuals periodically break off from their group and walk in a random path across the room, perhaps joining another group. If interactions between individuals in a group are very weak (on the order of k_BT), then there is only a tiny difference between the composition of the individuals inside the group and outside the group. When the interactions are sufficiently weak, all individuals in a group will disperse on a time scale much shorter than the duration of the party. Because this type of group exists only temporarily, it is termed a "fluctuation". On the other hand, if the interactions between individuals are strong, then groups persist for the duration of the party (although individuals continually join and leave their groups). In this case, each group is a "domain" and the composition of the people in a group is termed a "phase". The longer the tie line for this system, the larger the difference between the composition of individuals inside a group and outside that

group. When two domains of the same phase (i.e. two groups containing the same types of people) are jostled into contact with each other, they smoothly merge into one large group.

1.2.3.2 Fluorescence Microscopy to Identify Liquid Phases

Fig. 1 contains schematics of fluorescence micrographs of GUVs that correspond to some major points in the analogy. The vesicles contain different ratios of – at minimum – three lipids (namely, a phospholipid that melts at a high temperature, a phospholipid that melts at a low temperature, and cholesterol). Initially, the GUV is at an elevated temperature at which all lipids within the membrane are liquid and mix uniformly. At this high temperature, mixing entropy overwhelms interactions between different lipid types. As temperature decreases, lipid-lipid interactions gradually dominate over the mixing entropy. Small domains of one liquid phase nucleate within the initially uniform membrane.

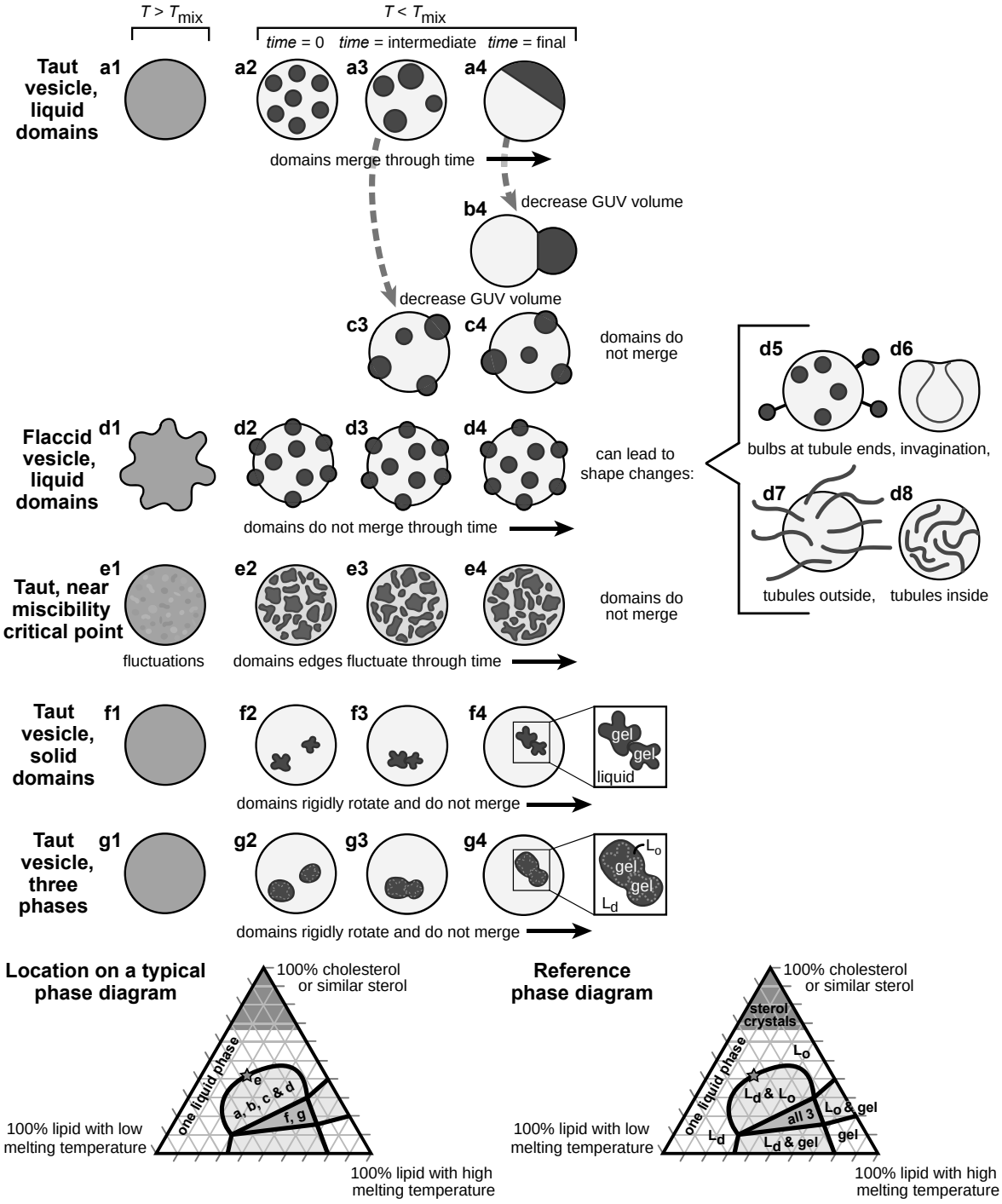

Figure 1 *from Box 18-1*:[11] Evolution of GUVs under various experimental conditions.

In experiments using fluorescence microscopy (see Chapter 10[20]), domains are visualized via the differential partitioning of a dye-labeled lipid, as in Fig. 2. Labeled lipids or hydrophobic environmental probes are incorporated into GUVs at trace amounts,[21–23] typically less than 1 mole percent. The primary requirement for a fluorescently labeled lipid is that it preferentially partitions between phases, giving rise to a contrast. The majority of labeled lipids partition preferentially into the least ordered membrane phase, even when the fluorophore labels a lipid that would be expected to partition preferentially into a more ordered membrane phase.[22,24–26] For example, fluorescently labeled cholesterol and saturated lipids typically partition to L_d phases rather than L_o phases, as do tail-labeled sphingolipids. Further illustrating the point that the designation of "ordered" and "disordered" is relative rather than absolute, the same fluorescent probe can partition to different phases under different conditions. For example, several probes partition to the ordered phase of giant plasma membrane vesicles (see Chapter 2 of [20]), but partition to the disordered phase of model GUVs produced from ternary mixtures of DOPC, brain sphingomyelin, and cholesterol.[26] In a different membrane system, a single probe has been found to switch its phase preference after crosslinking.[17]

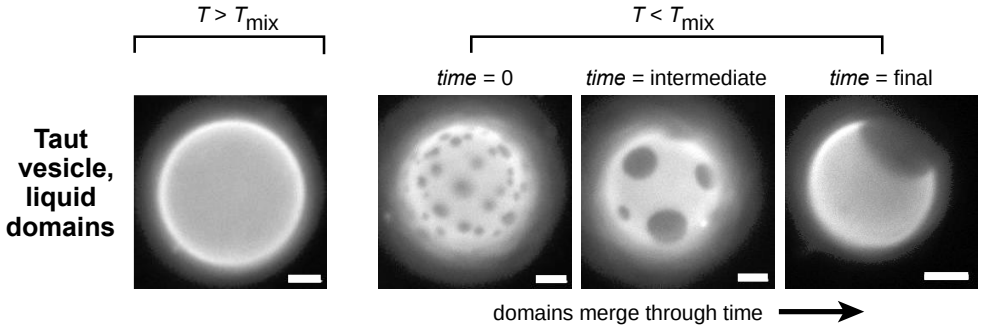

Fig. 2 *from Fig. 18-1.*[11] Representative micrographs of taut GUVs composed of 50/20/30 diphytanoylPC/DPPC/cholesterol, labeled with 0.8 mol% Texas red DPPE, which partitions preferentially to the L_d phase. At temperatures above T_{mix}, the vesicles are uniformly mixed. At temperatures below T_{mix}, two distinct liquid phases are observed. As time progresses, domains of each phase coalesce until

only one L_d domain and one L_o domain remain, corresponding to schematic a2-a4 in Fig. 1. The time scale for full coarsening is typically on the time scale of minutes to tens of minutes, and depends on the area fraction of each phase and the diffusion coefficients of domains.[27–29] Scale bars are 20 μm.

To characterize which phases are present in GUV membranes, it is useful to examine domain morphology and dynamics, as in the flow chart in Fig. 3. Liquid domains are typically circular, for the same reason that 3-dimensional liquid droplets are spherical. When GUV membranes demix into coexisting liquid phases, Brownian motion drives diffusion of the domains across the surface of the GUV.[30] When these liquid domains collide, they quickly and smoothly coalesce.[27,29,31] If the GUV membrane is sufficiently taut, then all domains of each liquid phase eventually merge until only one domain of the L_d phase and one domain of the L_o phase persist, as shown in a2-a4 of Figure 1 and in Figure 2. Researchers often choose to publish micrographs of GUVs as in panel a2-a3 (rather than in the final state of panel a4) because readers can immediately estimate the fraction of the GUV's area in each phase from a single micrograph. Estimating the area fractions in a single micrograph can be challenging if only one domain of each phase persists and if the unlabeled phase has very low fluorescence.

Fig. 18-2: Identification of coexisting membrane phases in GUVs by fluorescence microscopy

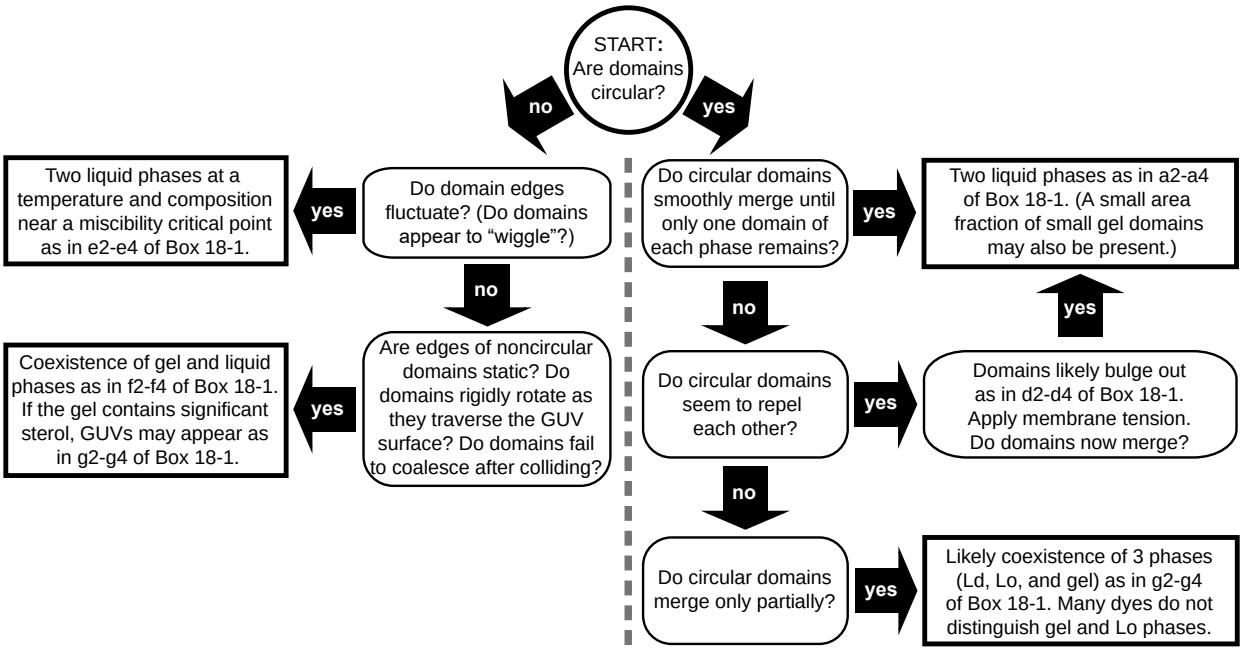

Fig. 3 *from Fig. 18-2*.[11] Flow chart depicting how to identify membrane phases in GUVs by fluorescence microscopy.

Exceptions exist to the rule that micron-scale liquid domains merge through time. One example occurs when vesicles are flaccid. Flaccid vesicles are said to have "excess area" such that the surface area of the membrane exceeds the area of a sphere with the same enclosed volume. In this case, domains are kinetically trapped from merging due to membrane curvature as in c3-c4 and d2-d4 of Fig. 1.[32–36] When the membrane has even more excess area, larger shape changes can occur, as in d5-d8 of Fig. 1. When these changes have a preferred orientation (e.g. tubules grow only toward the interior of a GUV), then the membrane has a non-zero spontaneous curvature and/or more material in one of the monolayer leaflets than the other. More commonly, tubules grow both outside and inside a single GUV.

Another example in which micron-scale domains do not merge occurs when the membrane composition and temperature are near a miscibility critical point as in e1-e4 of Fig. 1. We [the Keller lab] have previously reviewed the behavior of membranes near critical points.[37]

Above the critical temperature, non-circular composition fluctuations are observed through time in the membrane.[37–44] Below the critical temperature, domains boundaries fluctuate through time such that domains appear to wiggle.[39,45,46] The characteristic length scale of these fluctuations varies with temperature. Near the critical point, the fraction of the GUV's surface area covered by L_o phase and L_d phase membranes are nearly equal. The same phenomena have been observed in giant plasma membranes,[13] introduced in Chapter 2.[20]

1.2.3.3 Only Two Coexisting Liquid Phases Have Been Observed in GUVs

To date, a maximum of two coexisting liquid phases have been observed in a model lipid membrane at equilibrium, even when the membrane contains three or more lipid components. For example, only two fluorescence levels are observed in the GUVs in Fig. 2. This observation also holds in complex systems with a very large number of lipid types, such as giant plasma membrane vesicles in Chapter 2.[20,47–49] The Gibbs Phase Rule states that more coexisting phases are possible in this system, but are not required.

1.2.3.4 Fluorescence Microscopy to Identify Coexisting Gel and Liquid Phases

Gel phases are typically identified within GUV membranes as domains with non-circular shapes that do not change or relax over time. For many binary lipid systems, phase boundaries and tie lines derived from observation of GUVs can be compared to a decades-long history of data in which tie lines have been deduced from X-ray scattering of multilamellar vesicles (e.g. the work of Furuya and Mitsui in 1979).[50] Canonical examples of non-circular gel domains in GUV membranes appear widely in the literature.[21,51–54] Whereas liquid domains quickly relax to circular shapes in order to minimize line tension, reorganization of gel domains is not observed

on time scales accessible to most experiments due to slow lipid diffusion rates and intermolecular interactions that may result in lipid tilt with respect to the bilayer normal. Some gel phase domains have sharp, faceted edges, whereas others appear more curved and lobed like the two gel domains in f2 of Figure 1, especially if the GUV membrane contains cholesterol.

Gel domains nucleate within a liquid GUV membrane during a temperature quench. Individual gel domains are larger, and therefore easier to identify by microscopy, when the rate of cooling is slower, such that fewer gel domains are nucleated. In contrast to gel domains, liquid domains coarsen predominantly through a process of collision and coalescence (as in a2 – a4 of Fig. 1) to become several microns in diameter within seconds to minutes,[27,29] whether the rate of cooling is fast or slow.

Because some gel domains assume a circular shape, particularly if they contain significant fractions of cholesterol, observation of domains over time is a useful technique for determining membrane phases by fluorescence microscopy. When two gel domains come into contact through diffusion across the surface of a GUV, they do not merge. They may adhere to each other as shown in f2-f4 in Fig. 1, but the aggregate as a whole does not reorganize into a new shape on the time scale of experiments.

GUV membranes that contain three phases (L_o, L_d, and gel) can be challenging to identify by fluorescence microscopy for two reasons. First, the partitioning of most (but not all) lipidic dyes between the L_o and gel phases is indistinguishable. Second, in all reported instances in which all three phases coexist within a membrane, gel domains are found within L_o domains,[55] as depicted in g2 of Fig. 1. If a significant fraction of the membrane is in the L_o phase, then the difference between a domain that is entirely in a L_o phase and one that harbors a gel phase may not be obvious in a single micrograph.

To identify gel phases within L_o phases one can evaluate how domains change shape (or not) after they collide. If two colliding L_o domains each contains a domain of gel phase, then after the collision the two gel domains will not smoothly merge. Instead, the two gel domains will lie side-by-side, making an asymmetric structure. This structure will be coated by a single, merged L_o domain, as in g2-g4 of Fig. 1. If the total area of L_o phase is much larger than the total area of gel phase, then the merged domain in panel g3-g4 of Fig. 1 will appear circular, and it will be difficult to completely exclude the presence of gel phase. Complementary GUV imaging techniques, such as fluorescence lifetime imaging microscopy (FLIM) or the use of environmental probes such as Laurdan can also be useful in identifying phases.[55–57] Complementary techniques using geometries other than GUVs (e.g. nuclear magnetic resonance or electron paramagnetic resonance on multilamellar vesicles) produce excellent determinations of the lipid ratios and temperatures at which all three phases coexist.[38,58,59]

1.2.4 Advice and Pitfalls to Characterizing Phase Behavior in GUVs

The following section compiles technical hints that are particularly pertinent for researchers who are compiling phase diagrams of GUVs. These hints were discovered largely by trial and error by the community. Discussion of GUV preparation methods complements Chapter 1,[20] and discussion of imaging methods complements Chapter 10.[20]

Experimental problems can be especially challenging to recognize when vesicles form and undergo phase separation at a well-defined temperature that is shifted from the true transition temperature. The list of topics below is not exhaustive, and some appear in and/or are complemented by existing resources in the literature.[60–62] The list below highlights which

protocols we would check first when confronted with results that do not make sense, as well as the list of first suggestions that we would offer to a colleague encountering problems in the lab.

1.2.4.1 Compositional Variation

All methods of producing GUVs result in some variation in lipid ratio from vesicle to vesicle. As a result, every sample containing more than one GUV will produce a range of measurements of physical quantities such as transition temperature or area fractions centered at the "true" value, which is the transition temperature or area fraction of the average lipid composition of the population of GUVs.[60,63] This variation is exacerbated by the budding off of domains or tubes. The way that the community has reported experimental uncertainties in transition temperatures has evolved over the past decade. In the case of a GUV membrane demixing into coexisting L_o and L_d phases, the percentage of phase-separated vesicles varies sigmoidally with temperature, as in Figure 4, passing through 50% at the true transition temperature.[13,48,64,65]

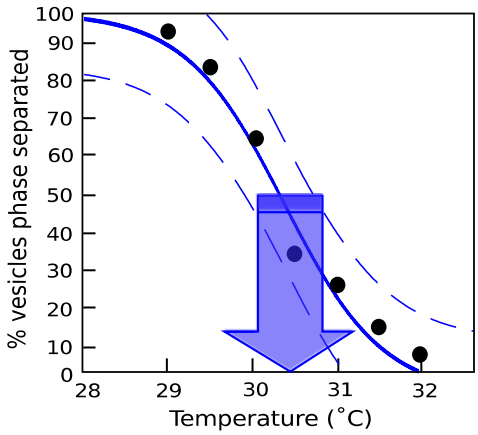

Fig. 4 *from Fig. 18-7.*[11] The black points, fit to a sigmoidal curve, represent the percentage of phase separated vesicles within a population of vesicles, versus temperature. All vesicles have the same nominal composition because they come from the same

sample. The vesicles were formed from a mixture of 35/35/30 DOPC:DPPC:cholesterol and labeled with 0.8 mol% Texas Red DPPE. The distribution of transition temperatures (the width of the sigmoid) is due to the distribution of vesicle lipid compositions. Dashed lines represent 95% confidence intervals from counting statistics.[65] The blue arrow points down to the miscibility transition temperature, where the width of the arrow is the experimental uncertainty.

Current best practice is to fit the sigmoidal curve with 95% confidence bounds given by counting statistics and to quote the uncertainty as the width of these bounds when 50% of GUVs have phase separated.[65] This uncertainty is smaller than the full width of the sigmoid, and shrinks as the number of vesicles in the sample set grows. The width of the sigmoid is affected both by the vesicle-to-vesicle variation in lipid ratio and by how sensitive the transition temperature is to changes in composition. That sensitivity varies across the phase diagram. Within a full phase diagram that probes many temperatures, the region of coexisting L_o and L_d phases is like a mountain with a flat top. A hiker walking across the flat top of the mountain changes latitude and longitude with little change in elevation. When that hiker encounters the steep side of the mountain, a small change in latitude or longitude results in a large change in elevation. Conversely, a small change in lipid ratio along a steep edge of the phase boundary results in a large experimental uncertainty. If a GUV sample produces a much larger range of transition temperatures than expected, then all subsequent data will be of low quality. The most expedient solution is to discard the sample and make new ones until the experimental uncertainty is consistently minimized.

1.2.4.2 Probes and Impurities

The addition of probes and impurities, especially hydrophobic and amphiphilic molecules, can shift transition temperatures in GUV membranes. To avoid the introduction of

plasticizers to membranes, chloroform solutions should be stored in and handled with glass or PTFE. Detergents should be thoroughly rinsed from all glassware. Glassware cleaned with acid should also be thoroughly rinsed. Some common solvents (e.g. ethanol) have been shown to alter membrane miscibility transition temperatures.[65,66] Fluorescent probes that strongly partition into one of two coexisting phases within a membrane also shift miscibility transition temperatures.[67] The probe Laurdan is generally thought to partition relatively equally between L_o and L_d phases and so presents a good alternative to probes that partition strongly.[21,68] A caveat is that determining partitioning of any dye is non-trivial because it is difficult to disentangle aggregation,[68] photoselection,[69] and other photophysical effects of the membrane on the dye from the dye's concentration. There are almost certainly cases in which C-Laurdan, a version of Laurdan with a carboxylic acid moiety,[69] does not partition equally between L_o and L_d phases. For example, when C-Laurdan is incorporated into giant plasma membrane vesicles or plasma membrane spheres, the difference in C-Laurdan intensities between the two phases is striking, whereas the difference in C-Laurdan signals between the L_o and L_d phases (the "difference in generalized polarization") is slight.[23,68,70]

1.2.4.3 Membrane Tension and Osmotic Pressure

Electroformation typically produces taut GUVs, which become flaccid over time. The effect of surface tension on miscibility transition temperatures in GUVs is small, only a few degrees over the range of tensions supported by a membrane without bursting.[71,72] In contrast, surface tension has an enormous effect on the rate of domain coarsening, as illustrated in Fig. 1. The use of osmotic pressure to apply (or relieve) tension likely introduces additional effects, given that osmotic pressure shifts membrane miscibility temperatures in an opposite direction

from tension applied by micropipette aspiration.[73] Because evaporation can occasionally occur in electroformation or gentle hydration chambers, even when they appear sealed, confirmation of osmotic pressures via direct measurement is prudent.

1.2.4.4 Photooxidation

Exposure to light can induce chemical changes in lipid molecules. Photooxidation changes the composition of GUVs by degrading the original lipids and by creating products that act as additional components. This shift in membrane composition can result in a shift in membrane phase behavior. For GUVs far from a miscibility phase transition, well within a region of the phase diagram with coexisting L_o and L_d phases, a hallmark of photooxidation is the nucleation of new small domains within pre-existing larger domains as in Fig. 5. The effect is equivalent to a slow temperature quench.[29] The process of photooxidation in lipid membranes has elicited significant attention in the literature, with researchers focusing both on how to minimize photooxidation and on how to intentionally harness it to induce or probe new membrane phase behavior,[54,62,74,75] as described more fully in Chapter 22.[20]

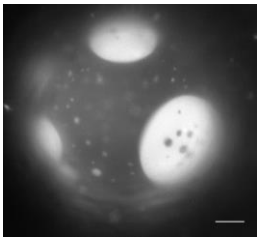

Fig. 5 *from Fig. 18-8.*[11] A representative micrograph of a photooxidized GUV composed of 35/35/30 DOPC:DPPC:cholesterol labeled with 0.8 mol% Texas red DPPE. Small, bright L_d domains are visible within the darker L_o region, and small, dark L_o domains are visible within large L_d domains. The large domains formed in the period after the initial temperature quench, and the small domains nucleated after an increase in the membrane's miscibility transition temperature, caused by photooxidation. Scale bar denotes 20 μm.

Whether photooxidation is perceived as a blight or a boon, it is most helpful to the scientific community if researchers quantify effects of light exposure in their experiments. For example, for GUVs composed of ternary mixtures of cholesterol and entirely saturated phospholipids, it is trivial to reduce the "measured drift in transition temperature due to photooxidation to at most –0.09˚C per exposure,"[39] which represents an inconsequential effect for most experiments. One way of quantitatively describing the effects of photooxidation is to quote the shift in GUV transition temperature from the beginning to the end of the experiment, for example by repeating a measurement on the same sample. Other ways to quantitatively describe those effects are to quote the number of visible domains nucleated (as in Fig. 5) per unit time at a constant temperature or to quote the change in area fraction over the course of an experiment at constant temperature. Given that domains that have recently nucleated are small, the former value is a much more sensitive measurement than the latter. For a population of GUVs in which the distribution of area fraction values is unusually narrow (~ 1%), quantifying the degree of photooxidation by measuring the change in area fraction over time produces a value that can readily be compared between laboratories.

For GUVs in which all phospholipid acyl chains are saturated, as in the example above, light exposure decreases miscibility transition temperatures in GUVs. For membranes comprised of at least one unsaturated phospholipid, light increases the same transition temperature, and the magnitude of the shift is larger. Lipids with polyunsaturated acyl chains are exquisitely vulnerable to photooxidation. In addition, the degree of photooxidation depends on the concentration and species of fluorophore in the system as well as the concentration of oxygen dissolved in the buffer.[67] Depending on the mechanism of photooxidation, a sample exposed to

light will continue to photooxidize after the light is shut off, and products of the photooxidation reaction can diffuse to regions outside the original area of illumination.

Because the degree of photooxidation is influenced by so many factors (e.g., the type of lipid, the type of probe, the type of solvent or substrate, and the degree of oxygen exposure), there are no universally recommended values for the maximum concentration of probe that should be incorporated in a GUV or the maximum number of photons per voxel that should be employed to image a GUV. A more broadly useful approach is to determine those maximum values, for each type of experiment in each laboratory, by assessing whether new domains nucleate or whether transition temperatures shift.

There are several strategies for mitigating the effects of photooxidation.[62] The simplest is to minimize the exposure to light. This includes (a) illuminating any individual sample for only a short time by frequently replacing the sample with new aliquots from the same vesicle preparation, (b) decreasing overall light levels, for example through the use of neutral density filters in a standard fluorescence microscope or through the use of lower laser intensity in a confocal microscope (especially for final measurements of transition temperatures in a new sample after an estimated transition temperature has been found in a sacrificial sample using higher light levels), (c) illuminating samples only when imaging, for example by using a shutter and short exposures, and (d) illuminating only the area of interest, for example by restricting illumination with an aperture or by using a light sheet microscope in order to illuminate only the focal plane through a GUV.[76] Other strategies include employing complementary imaging techniques such as differential interference contrast microscopy that does not require fluorescent probes, degasing aqueous solutions, preparing and imaging samples in an oxygen-free glove bag, and adding antioxidants to GUV solutions (which can themselves cause a shift in transition

temperatures).[54] The use of ITO-coated slides during electroformation of GUVs has been reported both to contribute to oxidation of lipids and to not be the dominant cause of shifts in membrane transition temperatures.[54,74]

Chemical assays can be used to verify the purity of lipid samples, but the common, semi-quantitative, method of thin layer chromatography (TLC) typically registers the presence of lipid contaminants only when their concentrations rise to a few mole percent. This level of sensitivity is not high enough for researchers to confidently assert that photooxidation has not significantly shifted phase boundaries in lipid membranes. As with any assay of impurities, a prudent approach is to intentionally add known amounts of impurities to a sample in order to gauge the concentration of impurity at which the assay registers a shift in the signal. Standardized versions of oxidized lipids are currently available commercially.

1.2.4.5 Substrate Interactions

Contact between GUVs and a substrate or other vesicles can shift transition temperatures and the spatial arrangement of domains. As usual, a best practice is to simply state the magnitude of the shift so that other researchers can assess if that offset will affect their own experiments. For example, miscibility transition temperatures of free floating GUVs and of supported bilayers produced by rupture of the same GUVs on a substrate differ by less than 5˚C for membranes of diphytanoylPC, DPPC,[77] and cholesterol. Similar studies found a shift in gel-liquid (main phase) transition temperatures of ≤ 2˚C.[78,79] When GUVs are in close contact with a surface, L_o domains tend to gather in the membrane at the contact area, such that the area fraction of domains on the remainder of the membrane appear depleted of L_o domains.[80,81]

1.2.5 Acknowledgements

During preparation of this chapter, the authors were supported in whole or in part by the National Institute of General Medical Sciences of the National Institutes of Health award 1F32GM115236 (to M.C.B.) and T32GM008268 (to C.C.), and by the National Science Foundation award MCB1402059 (to S.P.R. and S.L.K.). The authors thank Sarah L. Veatch for her comments on the manuscript, and Ilya Levental for sharing his expertise on C-laurdan.

1.3 Phase Separation in Giant Plasma Membrane Vesicles

Giant plasma membrane vesicles (GPMVs) are vesicles blebbed from a variety of cell types. These vesicles contain lipids and proteins from the original cell's plasma membrane and phase separate into coexisting liquid phases.[13,82] Interestingly, many GPMVs, from a variety of cell types, exhibit critical phase behavior.[13,82] There are several methods that induce GPMV formation and these various procedures are known to shift the miscibility transition temperature as well as the coarsening behavior of coexisting phases.[83] A noteworthy commonality between GPMVs and GUVs is the variation in membrane composition among a sample of vesicles from the same cell type.[13] This variation is at least partially due to the dependence of membrane composition on cell cycle phase.[84] GPMVs are limited as model systems for live cell membranes by the chemical changes, often in the form of crosslinking and reduction, induced by the blebbing procedure as well as the partial loss of asymmetry between the two leaflets of the membrane.[85]

1.4 Domains in Yeast Vacuoles

Micron-scale, protein-depleted regions along the vacuole membrane of the yeast *Saccharomyces cerevisiae* have been studied for decades.[86–90] Early freeze-fracture electron microscopy work indicated that the domains resulted from the membrane phase separating into coexisting liquid and gel phases.[91] More recent fluorescent microscopy work in unfixed, living cells, provides new evidence that the domains may be due to two coexisting liquid phases.[88]

Specifically, these studies found five pieces of evidence consistent with coexisting liquid phases. First, domains coarsen (domains of the same type merge followed by a perimeter rearrangement to minimize line tension).[92,10,93] A caveat to this observation is that domain coarsening was observed on a relatively long timescale (about ninety minutes), while coarsening is expected to occur on a seconds to tens-of-seconds timescale.[92,93] Second, around 25% of all vacuoles exhibiting domains had only one domain of each type, matching the expected equilibrium state for a fully coarsened phase-separated liquid-liquid system. Third, the domains persisted after proteolytic digestion of proteins on the cytoplasmic faces of isolated vacuoles, consistent with interactions between membrane component rather than interactions between cytosolic proteins. Fourth, only two types of domains are observed by both freeze-fracture and fluorescent labels (14 endogenous proteins and 2 lipid-sensitive dyes).[88,90,94,95] Finally, the fifth observation consistent with coexisting liquid phases is depletion of ergosterol from yeast reduces the number of vacuoles exhibiting domains. Sterols are a necessary membrane component to support coexisting liquid phases.[4] These observations are all consistent with coexisting liquid phases, rather than a liquid-gel coexistence.

Though these observations are consistent with liquid-liquid phase separation, they are not sufficient to conclude that observed domains are coexisting liquid phases. Indeed, the same paper

did not observe a change in domain morphology when temperature was raised to 55°C,[88] in direct contrast to the previous work of Moeller and Thomson who reported a gel-liquid phase transition around 40°C.[91] One possible explanation is that Moeller and Thomson experimented on fixed cells whereas Toulmay and Prinz imaged live cells and cell-free vacuoles. It is unclear whether chemical changes to membrane components due to fixation alter membrane phase behavior in yeast vacuoles.[85] In order to conclude that the domains in the membranes of yeast vacuoles are due to coexisting liquid phases, additional experiments are necessary to confirm there is a transition temperature above which the phases reversibly mix as well as the ability for domains of the same type to coarsen over time. I describe experiments of this type in Chapter 4.

1.5 Yeast as Model Organisms

Yeast are single-cell eukaryotes. The evolutionarily conserved similarities between the structure and function of proteins make yeast a viable model organism to better understand human cellular function. Yeast are easy to cultivate and propagate in lab and they have been used in laboratory settings longer than most eukaryotic organisms. The yeast *Saccharomyces cerevisiae* was the first eukaryote to have its genome fully sequenced,[96] is the eukaryotic organism whose genome and protein functions are most understood,[97] and exists in strains covering deletions for 90% of the genome and a plethora of mutations shared as standardized collections with labs around the world.[98,99] Any additional genetic variation is relatively easy to achieve due to established procedures that allow for precise genetic editing of the yeast genome.[97]

1.6 Yeast Nomenclature

Genes and Proteins. Naming conventions are organism-specific. Yeast genes and proteins share a three-letter code followed by a number. Genes are always italicized. They are further differentiated by being written in all caps if they are wild-type or dominant. They are written in all lower case if they are mutant or recessive. The proteins they encode are not italicized, have the first letter capitalized, and optionally append a "p" at the end. For example, in the case of the Vph1 protein:

VPH1	Wild type or dominant gene encoding the Vph1 protein
vph1	Mutant or recessive gene encoding the Vph1 protein
Vph1 or Vph1p	The protein itself

Table 1. Summary of naming conventions for yeast genes and proteins

Genotype. Yeast strains can vary greatly based on differences in alleles, mutations, and deletions, so it is vital to provide details on the genotype. The *MAT* allele can either be "a" or "alpha" and determines whether two yeast cells can mate sexually (they must have different *MAT* alleles to do so). A capital Greek delta, Δ, indicates a gene deletion. Further, numbers often follow this delta to detail how the deletion was achieved. A *Δ0* denotes a complete removal of the gene while other integers indicate the location where a deletion or mutation occurred that prevents the gene from being expressed. A dash "-" indicates a gene fusion, appending the following gene onto the preceding gene, such that V-W indicates the W gene is appended at the end of the V gene. Double semicolons indicate that the following gene has been inserted into the

preceding gene, so Y::X has X inserted into gene Y. Note that the location of insertion is not specified.

So, for example: *MATa his3Δ1 leu2Δ0 VPH1-GFP::HIS3MX6* tells us that a strain of yeast is mating type "a," capable of reproducing sexually with an "alpha" type yeast strain. The all lower-case genes followed by deltas indicate that there are two recessive and/or mutant genes (see "Genes and Proteins" above) deleted from this strain that encode histidine and leucine synthesis. The gene encoding leucine has been completely deleted while the gene for histidine production has either been partially deleted or mutated so that it is no longer functional. *VPH1-GFP* tells us that the dominant and/or wild-type gene encoding synthesis of green fluorescent protein has been fused onto the C-terminal end of the dominant and/or wild-type gene for Vph1 protein production. Further, a dominant and/or wild-type gene encoding histidine production has been inserted downstream of the *VPH1-GFP* fusion. Finally, the *HIS3MX6* cassette is a DNA module that uses PCR-based amplification to integrate the sequence into the yeast genome. It is good to note that the inclusion of *HIS3* on the cassette provides an easy experimental check for insertion: cells can be grown on a medium lacking histidine and only those cells that have successfully incorporated the *VPH1-GFP::HIS3* sequence will grow.

Yeast Strains. Naming conventions for yeast strains are less formalized. Best practice is to start with the alphanumeric code associated with the laboratory of origin followed by the genotype. For example, BY4741 *MATa met15Δ0 his3Δ1 ura2Δ0 leu2Δ0*, tells us that the yeast strain designated 4741 from Jef D. Boeke's lab (BY), is mating type "a," and has four mutant and/or recessive genes (encoding the synthesis of methionine, histidine, uracil, and leucine) deleted from its genome.

CHAPTER 2

Creating Diploid Cells

In order to make the vacuoles as large as possible, I attempted to make a diploid species of yeast. Ploidy refers to the number of sets of chromosomes contained within the cell(s) of an organism. *S. cerevisiae* commonly occurs as a haploid, that is, having one set of chromosomes, and procreates vegetatively by budding daughter cells without undergoing meiosis.[100] Yeast will respond to a mating hormone by reproducing sexually, giving rise to diploid cells that contain chromosomes from both parents.[100]

Yeast mate when they have different *MAT* alleles, either *MATa* or *MATα*.[100,102] Rather than depend on separate chromosomes, yeast mate when there are neighboring cells with the opposite *MAT* allele.[102] When these opposite alleles are active in two coexisting strains, they will mate in rich media.[102] In the case of yeast, diploid cells are ~1.3x larger than their parent haploids, with vacuole organelles also increasing in size and further fusing together into one, larger organelle.[101] I wanted larger vacuoles to increase the maximum size of domains, which are normally observed on the order of a few microns,[88] close to the resolution limit of standard epifluorescence microscopy.

I worked with a strain with a BY4742 genetic background, which is *MATα*. I mated this strain with the wild type strain BY4741, which is *MATa.* I streaked out one strain onto a YPD agarose plate and then streaked the second strain on top of it, being sure the streaks overlapped. I then grew the yeast for two days in a 30°C incubator.

To isolate diploid cells from any remaining haploid cells, I leveraged the fact that BY4742 and BY4741 have different auxotrophic characteristics. Strain genotypes are listed in

Table 2, with details on how to understand yeast nomenclature under Chapter 1, section 6 (1.6). I streaked the strain out first onto an agar plate with SC-met medium, medium that is similar to synthetic complete, except that it has no methionine amino acid. As a control, I also streaked out the two parent strains on the same plate. As expected, the wild-type BY4741 strain did not grow while the AMY1089 did along with the culture from my "mated" plate. I next streaked a sample of the "mated" cultures from this SC-met plate onto a SC-lys plate. As a control, I again streaked out the two parent strains alongside the "mated" culture. As expected, on the SC-lys plate, AMY1089 did not grow while both the BY4741 and mated cultures grew. Because the cells from the mated culture grow on both agar plates, I conclude that the cells are diploids containing the gene to create methionine from the AMY1089 chromosome and the gene to produce lysine from the BY4741 chromosome.

Strain ID	Base Strain	Genotype
AMY1089	Fields GFP library BY4742	*MATα his3Δ1 lys2Δ0 ura3Δ0 leu2Δ0 VPH1-GFP::HIS3MX6*
AMY79	BY4741	*MATa met15Δ0 his3Δ1 ura2Δ0 leu2Δ0*

Table 2. Summary of yeast strains used

CHAPTER 3

Thin Film Agarose Pads for HILO Illumination

Given a particular wavelength of light, HILO illumination increases the signal-to-noise ratio for a much greater sample depth than total internal reflectance.[103,104] However, signal increases the closer the sample is to the cover slip.[104] When working with intact cells, stationary cells in depleted media was placed directly onto glass cover slips. Cells free-fell until coming to rest on top of the glass cover slip. When working with cell-free vacuoles, we found that vacuole membranes rupture upon contact with glass. To prevent such rupture events, a thin film agarose pad was added to the coverslips.

Cell biologists have long made use of agarose pads to provide nutrients and cushion cells imaged over long periods of time.[105,106] Preparations of agarose pads vary and result in pad thicknesses that can range from tens of nanometers to a few millimeters. Thicker pads decrease the efficacy of HILO illumination. To prevent cell-free vacuole rupture while simultaneously bringing the vacuole membrane as close to the cover slip as possible, a thin film of agarose was deposited onto the coverslip.

Coverslips coated in a thin film of agarose were prepared by first cleaning the surface and then spin coating molten agarose onto the coverslip. Dust and other small particles were removed by wiping coverslips with ethanol-soaked Kimwipes. To remove any fibers left by the Kimwipe, the slides were then rinsed with ethanol. The coverslips were air dried and then placed in a plasma cleaner (Harrick, Ithaca, NY) for 3 minutes. The clean slides were then placed in a spin coater and spun for 1 minute at 4500 rpm. Once the spin cycle was started, 55 µL of molten 0.8% (w/v) agarose in PS buffer (10 mM Pipes-KOH pH 6.8 and 200 mM sorbitol) was pipetted

through a hole in the top of the spin coater. Adding the molten agarose after starting the spin cycle was necessary to create a coat of even thickness. This method does result in fingering of the agarose film, so it is vital to check each slide for sufficient coverage before use. Coverage can be checked by tilting the slide under a light. At the correct angle, the thin film is visible to the naked eye.

CHAPTER 4

Hallmarks of Reversible Separation of Living, Unperturbed Cell Membranes into Two Liquid Phases

4.0 Source

Sections 4.1-4.7 are taken verbatim from a manuscript accepted (2017) for publication in *Biophys. J.* Formatting, figure numbers, and refence numbers have been adjusted, but the content is otherwise identical. I was involved in all aspects of preparing this manuscript along with my co-authors Glennis E. Rayermann, Caitlin E. Cornell, Alex J. Merz, and Sarah L. Keller.

4.1 Abstract

The following is repeated from the thesis abstract on page 1

Controversy has long surrounded the question of whether spontaneous lateral demixing of membranes into coexisting liquid phases can organize proteins and lipids on micron scales within unperturbed, living cells. A clear answer hinges on observation of hallmarks of a reversible phase transition. Here, by directly imaging micron-scale membrane domains of yeast vacuoles both *in vivo* and cell-free, we demonstrate that the domains arise through a phase separation mechanism. The domains are large, have smooth boundaries, and can merge quickly, consistent with fluid phases. Moreover, the domains disappear above a distinct miscibility transition temperature (T_{mix}) and reappear below T_{mix}, over multiple heating and cooling cycles. Hence, large-scale membrane organization in living cells under physiologically relevant conditions can be controlled by tuning a single thermodynamic parameter.

4.2 Introduction

The first paragraph is repeated from the Introduction (section 1.1 general overview above)

Scientists have invested decades of effort in probing the lipid and protein composition of cell membranes for evidence of heterogeneity, which has the potential to control protein sorting, signal transduction, and other processes.[1] Aside from a few important exceptions, that extensive body of work has implied that the length scale of compositional heterogeneity in the membranes of unstimulated cells is limited to nanoscales.[2] Sub-micron domains in membranes gained notoriety as "rafts," and, more recently, as dynamic, short-lived "platforms."[2,3] These concepts are controversial because both terms are loosely or inconsistently defined, and because nanoscale domains are, at best, challenging to observe directly. In contrast to cell membranes, model lipid membranes spontaneously demix on large (μm) length scales, into two well-defined liquid phases. This demixing follows thermodynamic principles.[5,107] The concept of phase separation is subject to established, quantitative rules that enable rigorous verification of predictions. These rules apply equally well to simple bilayer membranes composed of only three types of lipids, to the complex bilayer membranes of giant plasma membrane vesicles blebbed from cells, and phase-separated cytoplasmic droplets recently implicated across a variety of cell biological activities.[6–8]

Tantalizing hints have been reported since the 1960s that living membranes are capable of separating into coexisting liquid phases, just as model membranes are. Pioneering experiments investigated the vacuole, the lysosomal organelle of budding yeast. Using freeze-fracture electron microscopy, Moor and Mühlethaler found that vacuole membranes of unfixed yeast contained domains depleted of large proteins.[86] Domains in vacuole membranes are physiologically regulated: large proteins are randomly distributed across vacuolar membranes in

the logarithmic phase of yeast growth, whereas protein-depleted domains appear when yeast are in the stationary phase (as nutrients are exhausted and the rate of cell division slows).[88–91,94] In many cases the domains in vacuole membranes are ~200 nm or larger, and are therefore resolvable using conventional optical microscopy.[88]

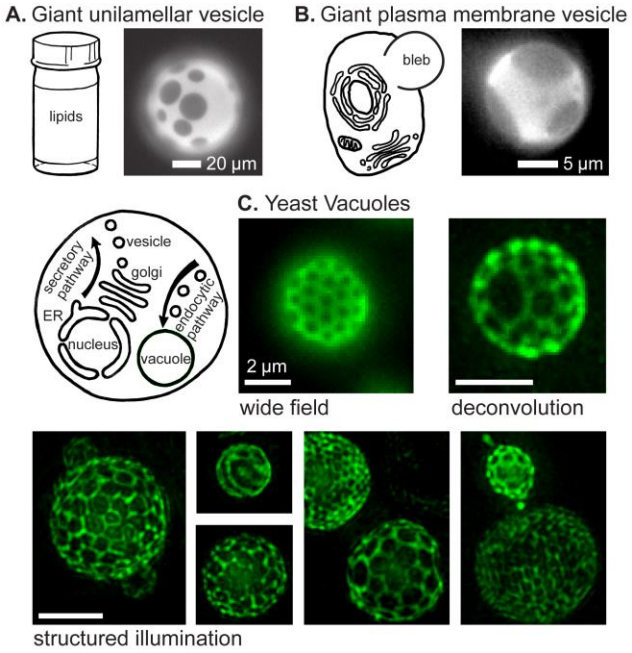

Fig. 6. *Fig. 1. of submitted manuscript*. Micron-scale, coexisting liquid phases appear in membranes of synthetic and biologically-derived model systems at equilibrium and in vacuole membranes of living yeast cells. **(A)** Giant unilamellar vesicles produced from ternary mixtures of synthetic lipids, imaged by standard epifluorescence. **(B)** Giant plasma membrane vesicles blebbed from adherent cells, imaged by standard epifluorescence. **(C)** Vacuoles within living yeast cells in the stationary phase of growth. Cells expressing a fluorescent vacuole membrane protein fusion (Vph1-GFP) were grown at 30 ˚C and imaged at ambient temperature (~22 ˚C) using either wide-field illumination on its own, wide-field illumination with z-z sectioning followed by iterative deconvolution, or structured illumination microscopy (3D-SIM) followed by iterative deconvolution. Information on the growth and imaging procedures is in the Methods. Scale bars in (C) = 2 µm.

The visual similarity of domains that form in both synthetic and cell-derived model membranes (Fig. 6*A* and *B*, respectively) to domains that form in yeast vacuole membrane domains *in vivo* (Fig. 6*C* and Fig. S1) is striking. In Fig 6*C*, contrast between the two domain types is provided by green fluorescent protein-tagged Vph1 (Vph1-GFP), an integral membrane subunit of the vacuolar proton (V-ATPase). Elegant experiments revealed that Vph1 is one of many proteins and lipids that segregate to one of the two domain types in vacuole membranes of living cells.[88] In recent work, the live cell results with Vph1 were unambiguously linked to the early freeze-fracture EM observations by immunogold labeling of freeze-fracture replicas.[90] In other words, freeze-fracture EM and optical microscopy of intact vacuoles in living cells observe exactly the same membrane structures.

Two hallmarks of a membrane separating into liquid phases are (i) coalescence of domains on short time scales and (ii) reversible mixing and demixing as a single thermodynamic parameter is varied. Previous attempts to observe these hallmarks in vacuole membranes have been inconclusive. Although multiple domains have been observed to merge into one larger domain, they did so on long time scales.[88] Similarly, although the fractions of mixed and demixed vacuole membranes have been observed to vary with temperature changes from 30˚C to 40˚C (by Moeller *et al.* in 1981),[91] subsequent research using live yeast reported that "vacuole structures did not visibly change when samples were visualized at a range of temperatures from 20 – 55˚C" (by Toulmay and Prinze in 2013).[88] Salient details of the early work are: the yeast were fixed before freeze-fracture, the fraction of vacuoles exhibiting domains decreased by one-third when the temperature of stationary phase yeast was increased from 30˚C to 40˚C, and that fraction recovered when temperature was returned to 30˚C.[91] The authors concluded that a solid (gel) phase transition had occurred.[91]

Additional observations are consistent with, but do not prove, that vacuole domains are due to membrane demixing into two coexisting liquid phases. (i) A variety of domain morphologies are evident in vacuole membranes, including pseudohexagonal arrays, stripes, and "half-moons" with only one large domain of each type.[88,89] (ii) Under the studied growth conditions, ~25% of vacuole membranes resembled half-moons.[88] (iii) On cell-free vacuoles, domains persisted after proteolytic digestion of proteins on the cytoplasmic faces of isolated vacuoles.[88] (iv) All labels used, which included 14 different endogenous protein markers and three lipid-sensitive probes, partitioned into one or the other of only two types of domains.[88,90] (v) Vacuoles typically contain 7-15 mole % sterol,[108,109] and the vacuole sterol content appears to increase during stationary phase.[90] When ergosterol (the major sterol of yeast membranes) is depleted with drugs or genetic manipulations, domain formation is impaired.[88–90] Synthetic membranes exhibit coexisting liquid phases only when one of their lipid components is a sterol such as ergosterol or cholesterol.[110] (vi) More broadly, several mutations that affect the lipid composition of vacuolar membranes result in the absence of membrane domains.[88–90] Domain formation is linked to the availability of lipids and sterols, from lipid esters stored in cytoplasmic lipid droplets, through a process called microlipophagy.[89,90,111] Although all six of these findings are consistent with the hypothesis that vacuole domains arise through phase separation, none of them presents a direct test.

We now test key predictions of the phase-separation hypothesis. If the phases are liquids, then domains are predicted to merge and rearrange on short time scales. If a miscibility transition occurs, the membranes are predicted to reversibly demix at a constant transition temperature. We conclude that vacuole domains exhibit hallmark behaviors of phase separation.

4.3 Materials and Methods

Table S3 in the *SI Appendix* lists methods and conditions for each figure and movie.

Synthetic membranes. GUVs were electroformed (19) and imaged as previously described (6, 20). In Fig. 1, Fig. S10, and Movie S8, the GUVs are composed of 35 mole% diphytanoyl-phosphatidylcholine (DiPhyPC), 35 mole% dipalmitoyl-phosphatidylcholine (Avanti Polar Lipids, Alabaster, AL) and 30 mole% cholesterol (Sigma, St. Louis, MO). The GUV in Fig. S2 is composed of 40 mole% di(13:0)-phosphatidylcholine, 20 mole% DiPhyPC, and 40 mole% cholesterol. All GUVs are labeled with 0.8 mole% Texas Red dipalmitoyl-phosphatidylethanolamine (TR-DPPE, Invitrogen, Carlsbad, CA).

Giant Plasma Membrane Vesicles. The vesicle in Fig. 1*B* was imaged at 10 ˚C under control conditions in (21).

Yeast cell culture. A BY4742 derivative, *MAT α his3Δ1 lys2Δ0 ura3Δ0 leu2Δ0 VPH1-GFP::HIS3MX6* was used. In general, when yeast are placed in fresh growth media, their growth follows a characteristic sequence of events. A "log phase" of rapid growth is followed by a "stationary phase" in which yeast vacuoles fuse to become as large as 5 μm in diameter (22, 23). Cultures (200 mL) were grown in synthetic complete (SC) media at 30°C in a shaking incubator for ~20 hours until the optical density (OD_{600}) of the culture was ~1.7, using 600 nm wavelength light. The culture was then grown an additional ~43 hours to reach the stationary phase, where the OD_{600} falls in the range of 6.8 – 7.8. This procedure is depicted in Fig. S7*B* and *C*.

Vph1-GFP fusion protein. Yeast vacuoles were labeled by fusing the Vph1 protein to green fluorescent protein (GFP), using homologous recombination. The fusion protein was expressed from the chromosomal *VPH1* locus under the native promoter, at normal cellular copy

number. The Vph1 fusions are known to retain physiological function and were previously shown to not spontaneously aggregate within the vacuole membrane, even during vacuole:vacuole docking (24). Vph1 has been shown to colocalize in yeast vacuoles to the same membrane domains as the fluorescent tracer FM4-64, which partitions preferentially to the liquid-disordered (L_d) phase in giant unilamellar vesicles (12).

Yeast imaging. Yeast are typically 5 – 10 μm in diameter, vacuoles are 3 – 5 μm, and domains in vacuole membranes are often close in size to the Abbe diffraction limit (~200 nm). Yeast were imaged by the four imaging techniques described in detail below. Image sequences collected by these techniques were then processed using a Kalman filter algorithm implemented in Image J (public domain http://rsbweb.nih.gov/ij/) to reduce detector and shot noise. For some experiments, yeast cells were adsorbed to coverslips coated with concanavalin A lectin (EPC Elastin Products Co.).

Imaging: Wide-field illumination. Yeast cells were imaged with an EMCCD camera on an Olympus IX71 fluorescence microscope as previously described, using a 60× 1.4 NA oil immersion objective (25). To reduce noise, multiple exposures were averaged. In the wide-field micrograph in Fig. 1*C* and all images of Fig. S1, eight consecutive 400 ms exposures were averaged. The micrographs in Fig. S3*B* were obtained by averaging four consecutive 200 ms exposures.

Imaging: HILO illumination (26, 27). To increase the signal-to-background ratio, yeast were imaged on a homebuilt Nikon Ti-U system with a 561-nm dipole-pumped solid state laser (MPB Communications, Pointe-Claire, QC, Canada). A Nikon CFI Plan Apo Lambda 100× 1.45 NA objective was used along with a dichroic quadband with 488/561/647/752 lines (Chroma)

and an ET605/70m filter. Images were acquired on an EMCCD (iXon Ultra 897, Andor) operating in frame transfer mode at 10 Hz, as described.[112]

Imaging: Deconvolution microscopy. Iteratively deconvolved wide-field sequences of images were acquired on a DeltaVision system (GE Healthcare) equipped with a CMOS camera and a 60× 1.40 NA objective (Olympus). Cell suspensions were introduced to homemade flow chambers made from #1.5 coverslips passivated with concanavalin A. Unbound cells were washed out with depleted media (taken from the supernatant of 1 ml of sample spun down at 1200 rpm for 2 min) or (for hypoosmotic shock experiments) with water. Z-stacks were acquired at 200 nm spacing at typically 0.15 s exposure per frame, and were deconvolved using SoftWorx software (GE Healthcare). From the deconvolved Z-stacks, brightest-point projections were computed. The projection time series datasets were then corrected for photobleaching using a histogram-matching algorithm implemented in ImageJ, and, finally, were Kalman filtered to reduce noise, also in ImageJ.

Imaging: Structured illumination microscopy. Samples were mounted as for deconvolution and imaged using an OMX-SR instrument (GE Healthcare) equipped with a 63× 1.42 NA objective (Olympus). The immersion oil refractive index was typically 1.516. Z-stacks were acquired at 120 nm spacing and images were deconvolved using the SoftWorx deconvolution package. Weiner spatial filter constants from 0.001 to 0.010 yielded similar reconstructions.

Imaging: Standard epifluorescence. Both the synthetic GUV membranes and blebbed GPMV membrane imaged in Fig. 1*A* and *B*, Fig. S2, Fig. S10, and Movie S8 were imaged as previously described.[6,13]

Thermal cycling. For both *in vivo* and cell-free yeast vacuole samples, temperature was controlled by air from a heat gun and monitored using a calibrated thermocouple. In experiments in which temperature data was collected, a graph is provided within the figures and, for the *in vivo* vacuoles, within the movies. Temperature data were collected with a thermocouple tip inserted between the coverslip and slide to make direct contact with the sample. The edges of the cover slip and slide were sealed with vacuum grease to prevent water loss due to evaporation. The synthetic membrane GUV shown in Fig. S10 and Movie S8 was temperature controlled as previously described, and the temperature was cycled about its miscibility transition temperature of 46.1°C.

Cell lysis to create cell-free vacuoles. Cells were harvested in a swinging-bucket rotor (3200 × g) for 10 min at room temperature, resuspended in 0.1 M Tris, pH 9.4, 10 mM DTT, and incubated for 10 min at 30°C. The cells were again sedimented in a swinging-bucket rotor (3200 × g) for 5 min at room temperature and then resuspended in spheroplast buffer (600 mM sorbitol, 50 mM potassium phosphate pH 7.5, and 8% v/v depleted media, saved from the first centrifugation step). Lytic enzyme (Zymolyase 20T, Seikigaku; further purified by ion exchange chromatography) was added to 3-fold higher concentration than in our standard vacuole prep (30) to adjust for cell wall composition in yeast grown into the stationary phase, and the cells were incubated for 1 h at 30°C. The spheroplasted cells were sedimented in a swinging-bucket rotor (3200 × g) for 5 min at 4°C. For hypoosmotic lysis, spheroplasts were resuspended in 15% ficoll buffer (10 mM Pipes-KOH pH 6.8, 200 mM sorbitol, and 15% w/v ficoll) and DEAE-dextran was added to a final concentration of 0.01% w/v. Spheroplasts were incubated for 2 min on ice, then 3 min at 30°C. The resulting spheroplast lysates were stored on a wet ice bath for no more than 4 hours before use.

Mounting cell-free vacuoles on slides. A thin agarose cushion was prepared by spin coating 55 µL of molten 0.8% (w/v) agarose in PS buffer (10 mM Pipes-KOH pH 6.8 and 200 mM sorbitol) on plasma-cleaned glass coverslips. Vacuole lysates were diluted 1:10 with molten 0.8% w/v low-melt agarose in PS buffer. The solution was mixed by gentle vortexing, deposited onto agarose-coated slides, and imaged by the same procedure as for living cells. Immobilization of vesicles within agarose gels does not affect the diffusion coefficient of individual lipids in vesicle membranes.[113]

Osmotic gradient. A simple flow cell was constructed from two coverslips joined along their edges by spacers of double-sided tape. The bottom coverslip was coated in concanavalin A. Yeast cells in their depleted media were drawn into the flow cell by capillary action and by wicking with paper. To induce hypoosmotic shock, a volume of deionized water, equal to the volume of sample loaded into the flow cell, was deposited at one end of the microfluidic chamber. Fluid was then wicked from the opposite end of the flow cell in order to introduce water into the flow cell.

4.4 Results and Discussion

The first hallmark of liquid phases that we observe in vacuole membranes is that two domains can coalesce on time scales of seconds. In synthetic GUVs with taut membranes, liquid domains diffuse freely over the vesicle surface, collide with other domains, and coalesce as in Fig. S2 until eventually only one domain of each type remains.[29] In synthetic GUVs with excess area (more area than necessary to enclose a spherical volume), domains in pseudohexagonal arrays are observed to bulge into or out of the vesicles and are hindered from colliding.[5,35,114,115] Similarly, the pseudohexagonal domains of yeast vacuoles have been observed to bulge inward

toward the vacuole lumen,[88,90,111] and fusion of these domains is a rare event. We hypothesized that domain collision in vacuoles might be triggered by applying a hypoosmotic gradient to yeast cells, which causes the vacuoles inside to swell due to internal turgor pressure. This was indeed the case: we capture rare events of domains colliding and quickly coalescing in Fig. 7, Fig. S3*A*, Movie S1 (played at 10x speed), and Movie S2 (played at 30x speed). We observe the reverse process in Fig. S4 and Movie S3 (played at 30x speed). During coalescence, the domain boundaries re-arrange to minimize the total length of domain interfaces. This is consistent with minimization of energy arising from line tension between the two membrane phases.

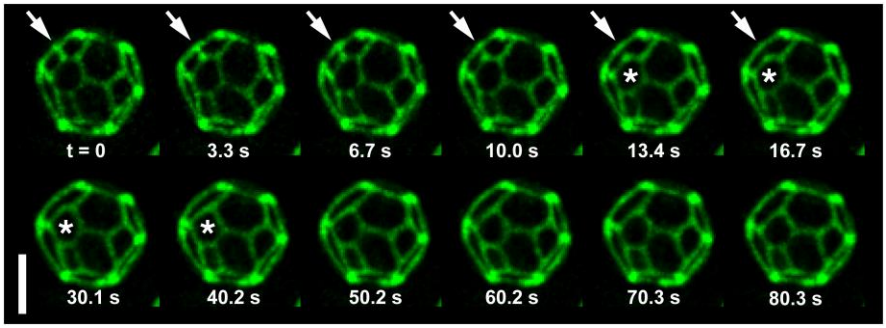

Fig. 7. *Fig. 2. of submitted manuscript.* Rapid coalescence of *in vivo* micron-scale domains in a single yeast vacuole membrane over time. Yeast cells were grown as in Fig. 6, mounted in a flow chamber, subjected to a hypoosmotic gradient, and imaged by z-sectioning and iterative deconvolution at ambient temperature (~23°C). Maximum brightness projections of the vacuole hemisphere closest to the microscope objective are presented. Arrows denote a region where two dark domains coalesce. Stars (*) denote a domain that changes shape from hexagon to pentagon, minimizing the total length of the domain interface. The scale bar indicates 2 μm. Movie S1 corresponds to the above sequence, played at 10x speed. The dynamic shift in the shape of the starred domain from a hexagon to a pentagon, from seconds 13.4 - 40.2 above, appear in seconds 1 - 4 of Movie S1.

Once the kinetic barrier for two domains to collide is overcome, coalescence of domains in yeast vacuoles occurs on the same time scale (seconds) as coalescence of domains that can be

an order of magnitude larger in synthetic vesicles.[29] This observation is consistent with the expectation that viscosities of yeast vacuole fluids, namely the cytoplasm and the vacuole contents (including high concentrations of polyphosphate), are higher than the viscosities of fluids used in synthetic GUVs.[116–118]

The second hallmark of liquid phases is the existence of a miscibility transition with respect to an intrinsic thermodynamic variable such as temperature, pressure, or membrane composition, as in the schematic in Fig. S5. Cyclic changes in any one of these thermodynamic variables cause domains to reversibly appear and disappear in synthetic vesicles.[4,119] To test whether the domains in yeast vacuole membranes arise from demixing of a single liquid phase into two coexisting liquid phases, we subject yeast to rapid temperature cycles.

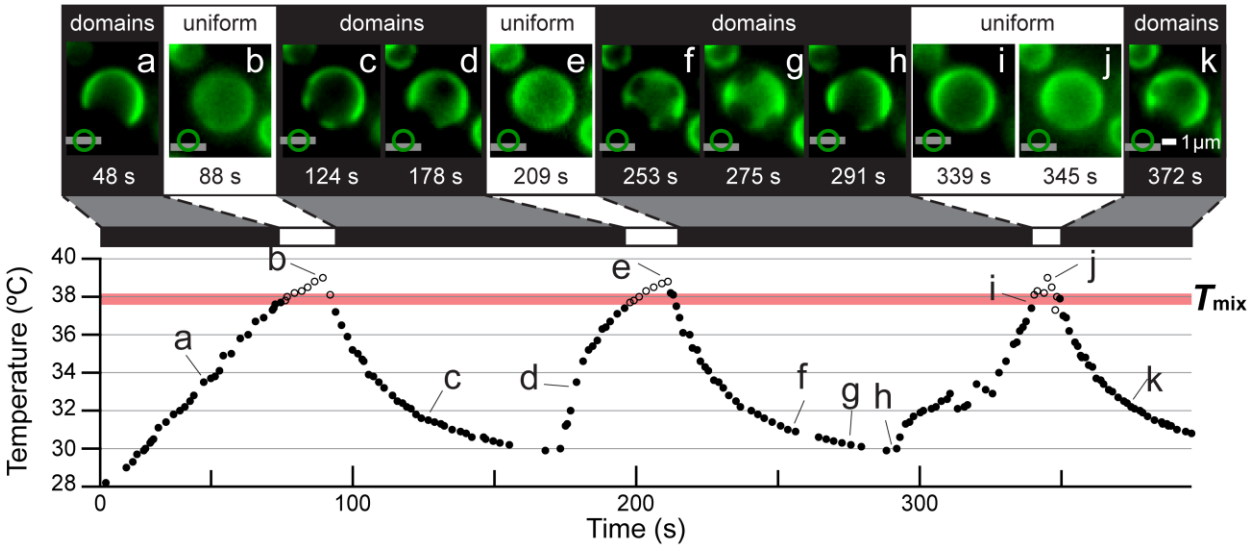

Fig. 8. *Fig. 3. of the submitted manuscript.* Micron-scale domains in an *in vivo* yeast vacuole reversibly vanish and reemerge through three temperature cycles. Micrographs *a*, representing 48 seconds, through *k*, representing 372 seconds, correspond to the labeled locations in the plot of temperature vs. time. A symbol illustrating the focal plane (grey line) at either the top, equator, or bottom of the vacuole (green circle) specifies the focal plane at which the vacuole was imaged in each micrograph. The temperature at which open

> symbols on the graph change to filled symbols (and *vice versa*) is T_{mix}. A thick, horizontal red line is drawn to highlight the transitions; the line is not a statistical fit. Vacuoles were imaged using HILO illumination. Movie S4 corresponding to this figure appears in the *SI Appendix* and plays at 3x speed such that micrograph *a* appears at 16 seconds in Movie S4 and micrograph *k* appears at 2 minutes and 4 seconds.

In Fig. 8, Fig. S6, and Movies S4 and S5 (both played at 3x speed), we cycle the temperature of yeast cells in the stationary phase of cell growth. At the standard growth temperature of 30 ˚C, yeast vacuoles exhibit dark domains on a bright background marked by GFP-Vph1 (Fig. 6*C*). At temperatures above ~37 ˚C, the domains disappear and the membrane is uniformly labeled.

Electron-microscopy results show that large proteins within a uniformly labeled membrane are randomly distributed across the entire membrane.[90] Upon cooling of membranes, domains nucleate and are large enough to image within seconds. For comparison, transcription and translation in yeast occur on timescales of at least minutes. The ability of the vacuole membrane to abruptly and reversibly switch between two states (namely, the presence and absence of domains), at a distinct temperature, and over multiple heating and cooling cycles, is a defining feature of a phase transition.

Cell viability is not affected by the temperature cycling regime used here (Fig. S7*A* and Tables S1 and S2). Moreover, individual yeast cells that exhibit domains in their vacuole membranes successfully grow and undergo mitosis when supplied with fresh nutrients.[88] Within a population of yeast cells, the T_{mix} of the vacuole membrane varies from cell to cell, just as it does in plasma membrane vesicles,[84] as might be expected for any biological parameter regulated by an array of biochemical and physiological variables.

To verify that the cyclical disappearance and reappearance of vacuole domains is intrinsic to the membrane rather than originating in the yeast cytoplasm, we extended the results of Fig. 8 to cell-free vacuoles. Fig. 9, Fig. S8, and Movie S6 (played at 3x speed) show that domains in cell-free vacuoles reversibly vanish and reappear as the temperature is cycled. The location at which domains reappear depends on the speed of cycling. When temperature is *quickly* cycled (as occurred in Fig. 8 and in Fig. S8-top, Fig. S9-rapid, and Movie S7, which plays at 3x speed), domains disappear and re-nucleate at approximately the same positions on the vacuole. The same effect occurs when synthetic GUVs undergo rapid temperature cycling (as in Fig. S10 and Movie S8, which plays at 10x speed). This is because as the temperature increases, domains disappear through a process in which the edge blurs, as in Movie S5 (played at 3x speed); domains do not disappear by becoming continually smaller. Edge blurring is expected when labeled molecules are suddenly free to diffuse over the entire surface of the membrane. When the temperature is held above T_{mix} for longer periods, such that lipids and proteins have ample time to diffuse across the membrane and mix uniformly, domains nucleate at new positions, both on vacuoles (Fig. 9, Fig. S8-bottom, Fig. S9, and Movie S9-slow, which plays at 3x speed) and on synthetic vesicles (Fig. S10 and Movie S8, which plays at 10x speed). In the language of condensed matter physics, this behavior is consistent with domains arising through a mechanism of nucleation and growth rather than with fluctuations arising through a mechanism of spinodal decomposition of a membrane poised near a miscibility critical point.[6,13]

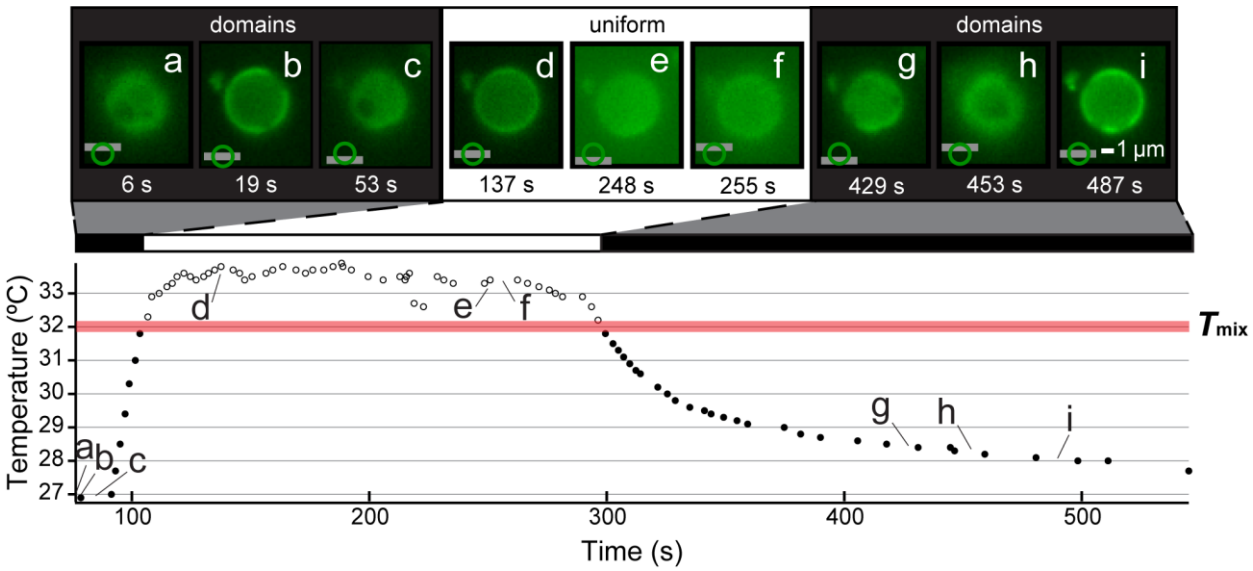

Fig. 9. *Fig. 4 of submitted manuscript.* Micron-scale domains in a cell-free yeast vacuole reversibly vanish and reappear through temperature cycles. This figure is one of three cycles in Fig. S8. Micrographs *a* through *i* correspond to the labeled locations in the plot of temperature vs. time. Other details are as described for Fig. 8. Movie S6 corresponding to this figure appears in the *SI Appendix* and plays at 3x speed; such that micrograph *a* appears at 2.1 seconds in Movie S6 and micrograph *i* appears at 2 minutes and 42.5 seconds. Preparation of cell-free vacuoles is described in the Methods section.

The location of domains in vacuole membranes does not appear to be governed by static protein scaffolds. By mass, about half of the vacuole membrane is protein, comparable to ~70% for a plasma membrane.[108] Although vacuole membranes may be associated with protein scaffolds, we observe that domains have variable sizes, move across the surface of vacuoles, smoothly and quickly coalescence into larger domains, and re-nucleate in new locations. In addition, domains persist after digestion of proteins on the cytoplasmic face of isolated vacuoles.[88] All of these properties are inconsistent with domain edges constrained by static scaffolds.

The coalescence of small domains into larger ones followed by reorganization of domain edges within yeast vacuole membranes (as in the starred domain in Fig. 7) implies that the

domains result from a miscibility phase transition rather than from the extensive crosslinking used to induce micron-scale domains in stimulated cell membranes,[2] from cell polarization,[120–122] from vacuolar fragmentation or deep invaginations due to hyperosmotic stress,[123] or from the regulated assembly of contacts between docked yeast vacuoles.[124,125] Neither the presence nor the absence of domains is perturbed by ATP depletion.[88] We can also rule out contact between lipid droplets and vacuoles as a *direct* driver of vacuole domain formation because only a subset of the domains in vacuole membranes correlates with the presence of docked lipid droplets.[89,90,111] The presence of many more domains than droplets requires an additional mechanism, such as phase separation. The localized release of sterols into the vacuole membrane through microlipophagy of docked lipid droplets, via the Npc1/2 system,[89,90,111] appears to be an indirect driver of phase separation across the entire membrane. Finally, we note that the assembly of docking domains prior to bilayer-bilayer fusion is consistent with and may be driven by membrane phase behavior.[124–126]

4.5 Conclusion

Here we show that large-scale membrane organization in yeast vacuoles is the result of demixing of the membrane into coexisting liquid phases and that this demixing is fully reversible. This mechanism operates in live cells imaged using non-invasive methods. In model vesicle membranes, demixing occurs equally upon a change in temperature or membrane composition. At constant temperature, cells may regulate membrane phase separation in response to external or internal cues. For example, the NPC1/2 cholesterol transport system controls domain formation.[90] Moreover, the Slt2/Mpk1 kinase is essential for the formation of phase-separated domains in the yeast vacuole.[88] Previously, [the Merz lab] demonstrated that

Slt2, a key node in the protein kinase C (PKC)-Rho1 signaling pathway, regulates both lipid acyl chain composition and bilayer fluidity.[127] Knowledge that vacuole membranes reversibly demix into coexisting liquid phases enables direct application of physical rules of membrane phase behavior established in model systems to living biological membranes. Description of domains as arising from a mechanism of phase separation rather than as less well defined "raft-like"[90] domains provides a tractable paradigm for future investigations of the regulation and mechanisms of *in vivo* membrane domain partitioning.

4.6 Acknowledgements

This material is based upon work supported by the National Science Foundation (NSF) Graduate Research Fellowship Program under Grant No. DGE-1256082 to G.E.R., by NSF MCB-1402059MCB-07444852 to S.L.K., by the National Institute of General Medical Sciences of the National Institutes of Health (NIH) under award T32GM008268 to C.E.C., and by NIH GM077349 to A.J.M. We thank Liz Manrao, Dan Nickerson, Rachael Plemel, Tyler Chozinski, Marco Howard, Lauren Gagnon, and Aaron Halpern for technical advice. Micrographs provided by Ellyn Gray and Sarah Veatch (Fig. 1B), and Joan Bleecker (Fig. S2) are used with permission. We are grateful to Prof. L. Wordeman for providing microscope time.

4.7 Supporting Material

The following is reproduced verbatim from the Supporting Information document accompanying our submitted manuscript and contains Figs. S1 to S10, Tables S1 to S3, and Captions for Movies S1 to S9. Movie files S1 to S9. References to manuscript figures have been updated to match the rest of this document.

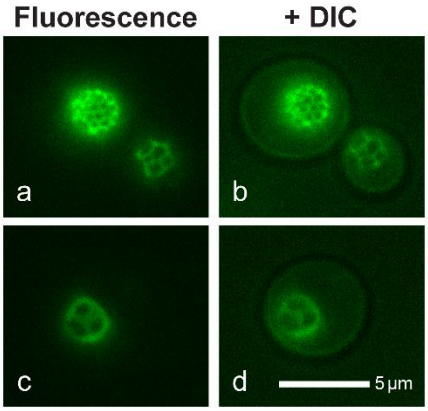

Fig. S1.
In the stationary phase of growth, yeast cells typically contain only one large vacuole. In panels **a** and **c**, yeast cells are imaged by wide-field illumination. In panels **b** and **d**, overlay composites show both wide-field illumination and differential interference contrast microscopy (DIC) to reveal the outline of the whole cell. All vacuoles in this figure exhibit membrane domains.

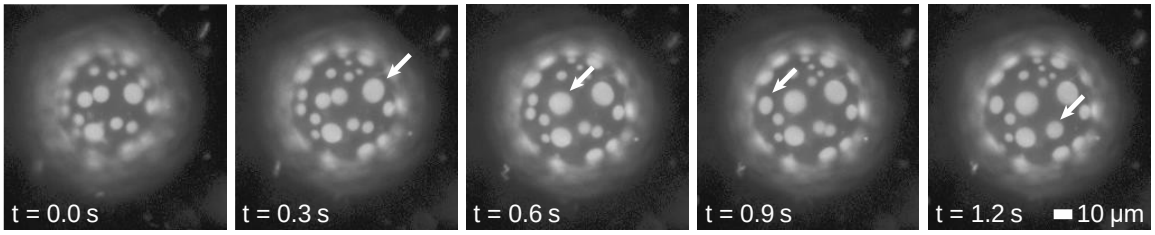

Fig. S2.
Micron-scale, liquid domains on the surface of a model giant unilamellar vesicle (GUV) collide and coalesce. Coalescence of liquid domains occurs when the membrane has no excess area (i.e. when it has no more area than is needed to cover the surface of a sphere with the interior volume). Arrows show single domains that had previously appeared as two separate domains in the preceding frame of the video. As time progresses, all domains eventually merge until the vesicle has only one domain of each type (not shown). As an analogy to explain why coalescence is characteristic of separation of two liquid phases, consider a bulk mixture of two immiscible liquids like oil and water. When the mixture is shaken, droplets of oil disperse within the water. With time, the droplets coalesce until all the oil lies in a separate layer on top of the water. Images provided by Joan Bleecker and used with permission.

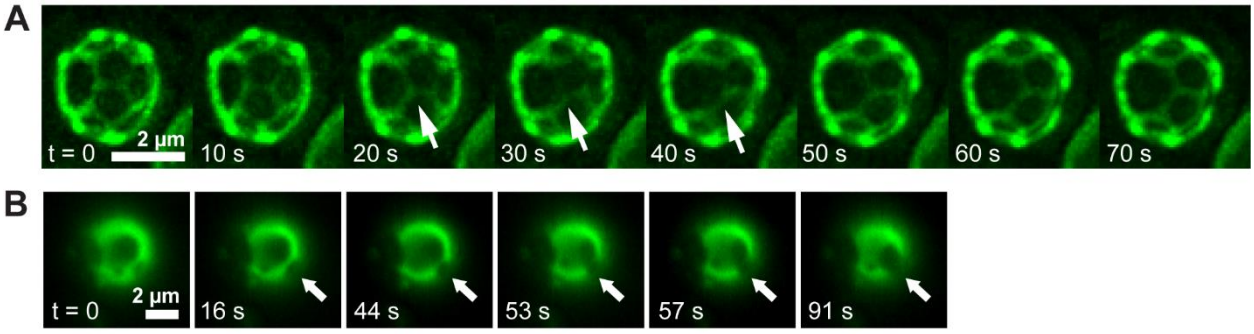

Fig. S3.
Coalescence of micron-scale domains in the membranes of two *in vivo* yeast vacuoles over time at a constant temperature. The vacuoles were inside yeast cells in the stationary phase of growth as in Fig. S1. The images in **A** result from deconvolution of twelve Z–sections of the top hemisphere of the vacuole. The arrows indicate a region in which two domains begin to coalesce. Movie S2 corresponds to this set of images and is played at 30x speed. The images in **B** were captured by wide-field illumination. The arrows point to a region where two domains diffuse into contact with each other, collide, and coalesce.

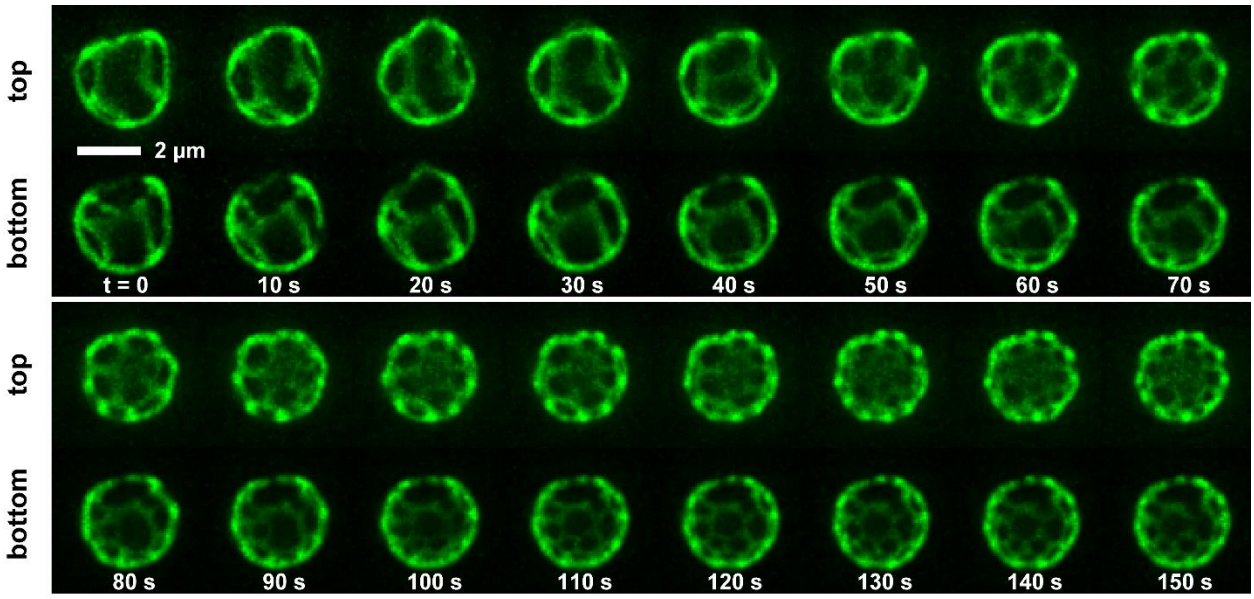

Fig. S4.
The *in vivo* liquid domains in a yeast vacuole sometimes become smaller after osmotic gradients are applied to yeast cells. At each time interval, z-sections were acquired and iteratively deconvolved. Renderings correspond to the two hemispheres of the vacuole, labeled as top and bottom. Movie S3 corresponds to this figure and is played at 30x speed.

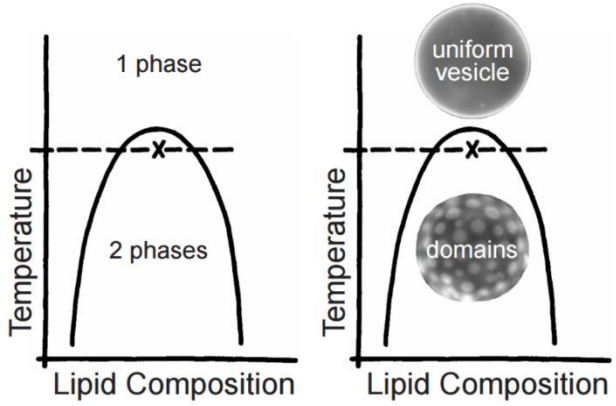

Fig. S5.

Schematic for coexistence behavior of two liquid phases in a synthetic membrane of a giant unilamellar vesicle. Vesicle images correspond to a membrane with lipid composition x shown on the figure. For all temperatures and compositions that fall within the curve, the membrane demixes into two liquid phases. Specifically, domains nucleate and grow through a process of collision and coalescence (as shown in Fig. S2). Outside the curve, the membrane is in one, fully mixed phase. Changes in thermodynamic variables, such as composition or temperature, result in a phase transition from one regime to another.

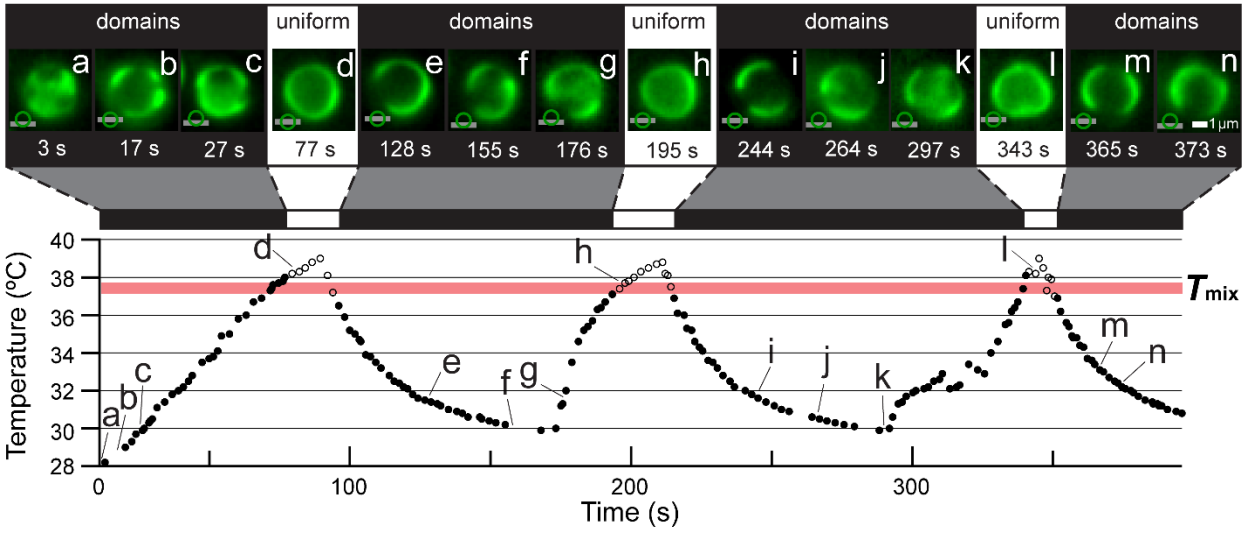

Fig. S6.

Micron-scale domains *in vivo* in a yeast vacuole reversibly appear and vanish through multiple temperature cycles. Micrographs *a* through *n* correspond to the labeled locations in the plot of temperature vs. time. A symbol illustrating the focal plane (grey line) at either the top, equator, or bottom of the vacuole (green circle) specifies the focal plane at which the vacuole was imaged in each micrograph. Several micrographs were recorded at times that fall between temperature points. Open symbols indicate that the vacuole was uniform; filled symbols indicate micron-scale domains. The temperature at which open symbols on the graph transition to filled (and *vice versa*) is T_{mix}. A thick, horizontal red line is drawn to highlight the transitions; the line is not a statistical fit. Imaged by HILO illumination. Movie S5 corresponds to this figure and plays at 3x speed such that micrograph *a* appears at 1 second in Movie S5 and micrograph *n* appears at 2 minutes and 4.3 seconds.

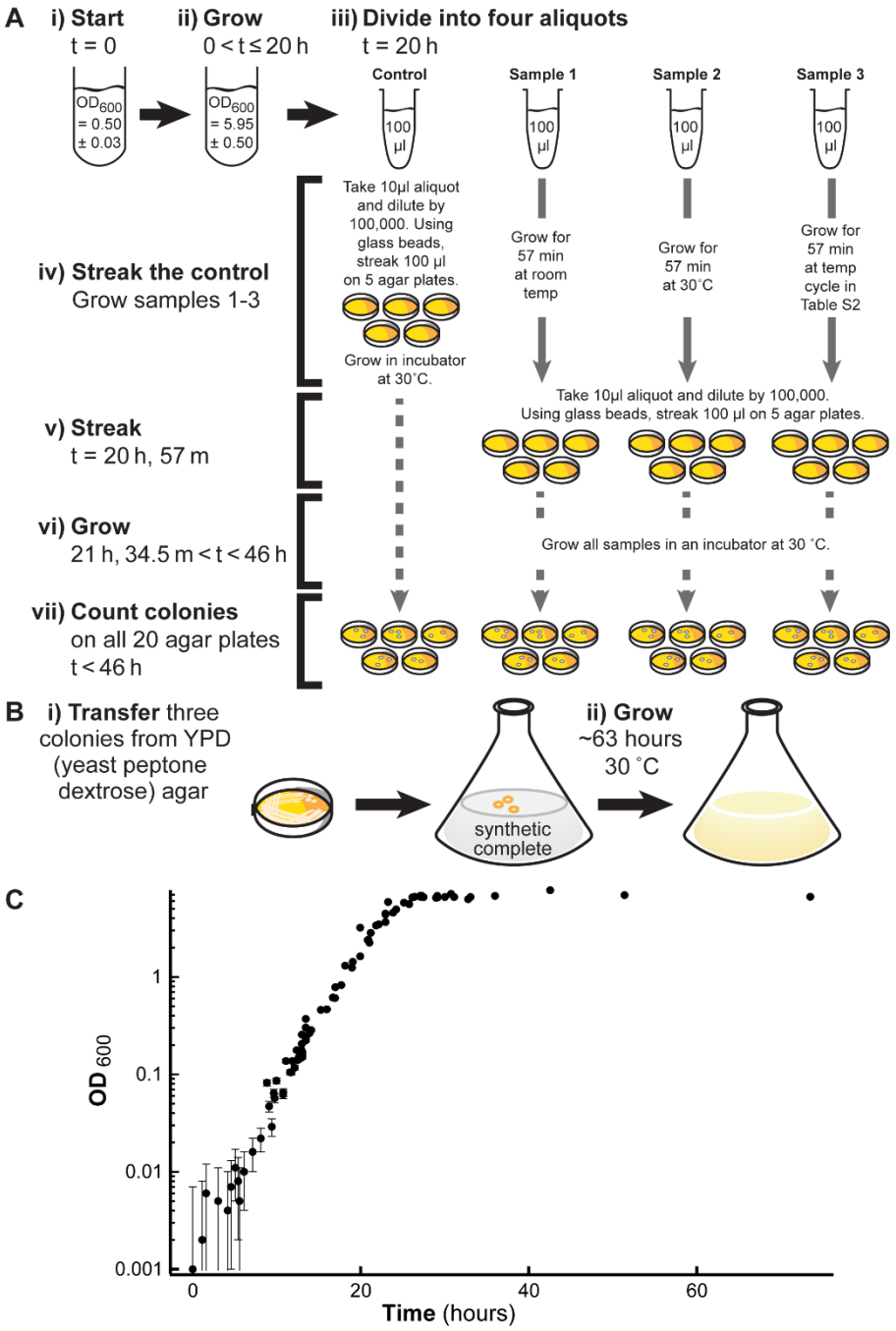

Fig. S7.

(A) Protocol for yeast viability experiment (results in Table S1). (B) Growth protocol to grow 3 colonies of yeast in 200 mL of media for ~63 hours. (C) Growth curve of the yeast in this study, where OD_{600} is the optical density at 600 nm as described in the methods of the main text. Error bars are based on the variation in OD_{600} readings for media blanks.

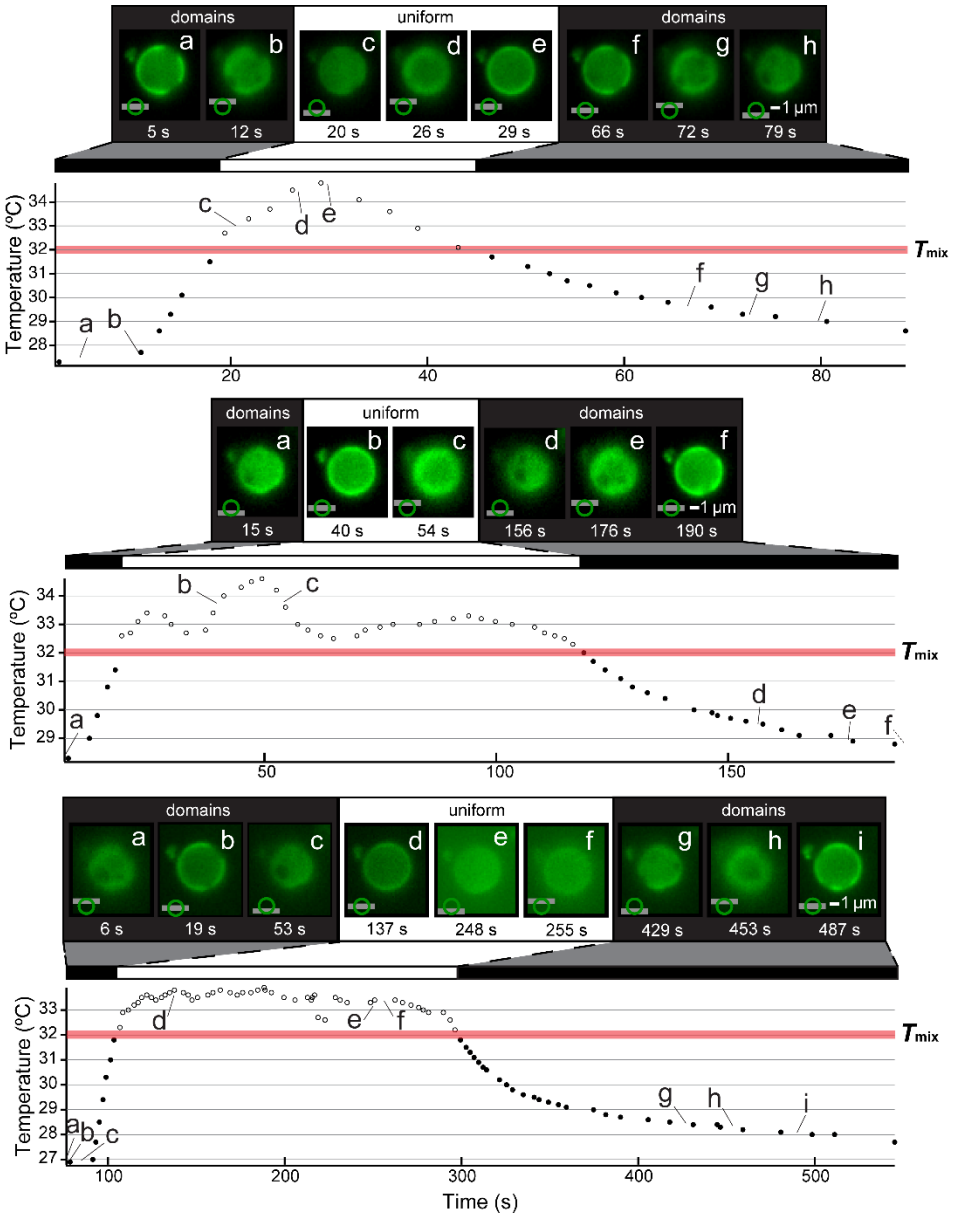

Fig. S8.

Micron-scale domains in a cell-free yeast vacuole reversibly vanish and reappear through multiple temperature cycles. Lowercase letters (e.g. *a* through *i*) correspond to labeled locations in the plots of temperature vs. time. A symbol illustrating the focal plane (grey line) at either the top, equator, or bottom of the vacuole (green circle) specifies the focal plane at which the vacuole was imaged in each micrograph. Open symbols indicate that the vacuole was uniform; filled symbols indicate micron-scale domains. The temperature at which open symbols on the graph transition to filled symbols (and *vice versa*) is T_{mix}. A thick, horizontal red line is drawn to highlight the transitions; the line is not a statistical fit. Imaged by HILO illumination. The bottom panel of this figure corresponds to Fig. 9 of the main text and to Movie S6, which is played at 3x speed.

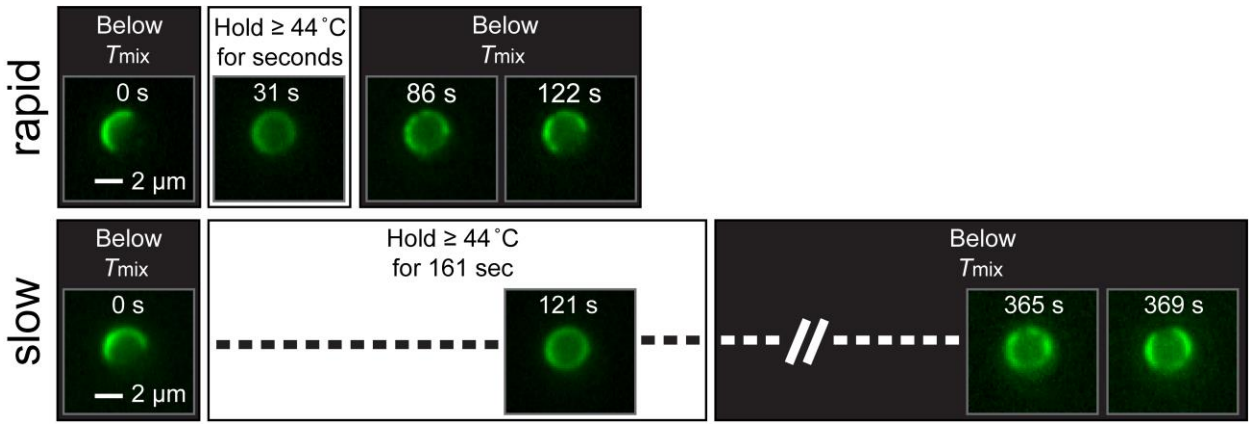

Fig. S9.

Examples of rapid and slow temperature cycling of a vacuole in a single yeast cell. The top line of images shows rapid cycling. Movie S7 corresponds to this top line and plays at 3x speed. The vacuole begins below T_{mix} and has a single large domain. The temperature increases monotonically for ~30 s [~10 s in Movie S7], when the vacuole reaches a temperature above T_{mix} and appears uniform. At 86 s [~28 s in Movie S7], temperature has returned below T_{mix} and domains are visible again. This sequence of images demonstrates that after rapid cycling, domains re-nucleate primarily at the same locations on the surface of the vacuole from which they disappeared, resulting in domain distributions at 122 s [~41 s in Movie S7] similar to the original distribution at 0 seconds.

In the bottom line of images, the same temperature cycle is executed more slowly. Movie S9 corresponds to this bottom line and plays at 3x speed. The vacuole is held above T_{mix} for a time that is sufficiently long (> 2 min) for membrane components to mix more uniformly. As a result, when the temperature is lowered below T_{mix} again, smaller domains nucleate at different locations on the surface of the membrane from which they previously disappeared, as shown in the image at 365 s [~122 s in Movie S9] and at 369 s [123 s in Movie S9]. HILO illumination was used to acquire the images.

These concepts are illustrated again in the GUV in Fig. S10 and Movie S8, which plays at 10x speed.

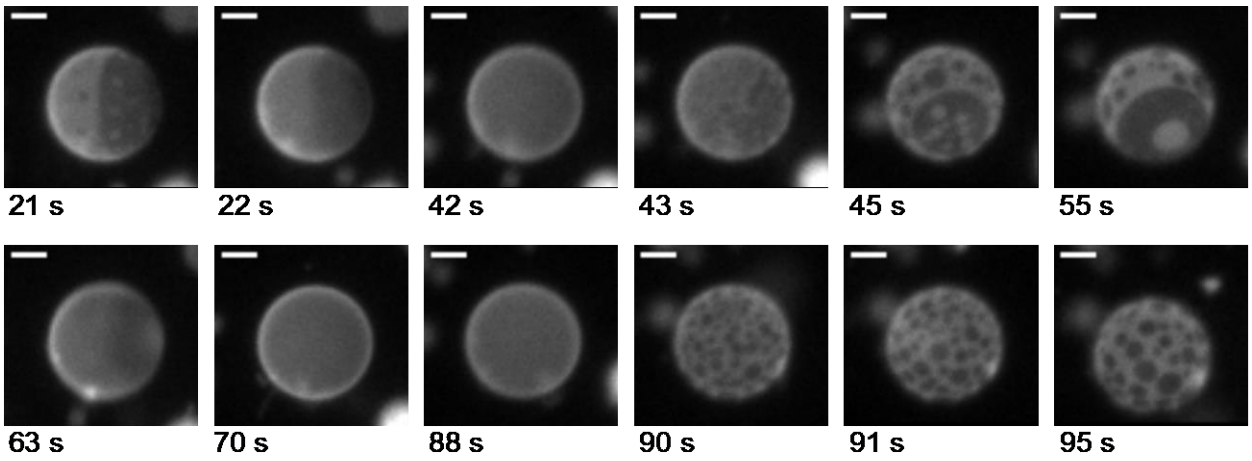

Fig. S10.
Fluorescence microscopy images showing reversible phase separation in a membrane of a single, synthetic, giant unilamellar vesicle (GUV) through time as temperature is cycled. Movie S8 corresponds to this figure and plays at 10x speed; time points in the movie are listed in square brackets []. In the top line, temperature is quickly cycled from below T_{mix} (at 21 s [2.1 s in Movie S8], when large domains are visible) to above T_{mix} (at 42 s [4.2 s], when sharp domain boundaries can no longer be distinguished), to below T_{mix} again (at 43 s [4.3 s]). This sequence of images demonstrates that after rapid cycling, domains re-nucleate (at 43 s [4.3 s]) primarily at the same locations on the surface of the GUV from which they disappeared, resulting in domain distributions (at 55 s [5.5 s]) similar to the original distributions (at 21 s [2.1 s]).

In contrast, in the bottom line, the same temperature cycle is repeated more slowly in the same GUV. At 55 s [5.5 s in Movie S8], the GUV membrane is below T_{mix} and has large domains. At 63 s [6.3 s], the GUV is above T_{mix} and sharp domain boundaries can no longer be distinguished. The GUV is held above T_{mix} for a time that is sufficiently long for all membrane components to mix uniformly (until 88 s [8.8 s]). As a result, when the temperature is lowered below T_{mix} again, small domains nucleate over the entire surface of the vesicle, as shown in the image at 90 s [9 s]. Those domains grow by collision and coalescence over time (as in Fig. S2), resulting in the image at 95 s [9.5 s]. The scale bar is 20 μm.

	Control:	**Sample 1:** Grown at room temp (~22 ˚C)	**Sample 2:** Grown at 30 ˚C	**Sample 3:** Grown with temp. cycle
Trial 1, Plate 1	87	101	77	101
Trial 1, Plate 2	108	97	109	102
Trial 1, Plate 3	99	79	133	85
Trial 1, Plate 4	84	113	110	61
Trial 1, Plate 5	99	105	109	133
Trial 1				
Average ± S.D.	**95 ± 10**	**99 ± 13**	**108 ± 20**	**96 ± 26**
Trial 2, Plate 1	110	110	99	122
Trial 2, Plate 2	68	101	85	119
Trial 2, Plate 3	111	99	106	116
Trial 2				
Average ± S.D.	**96 ± 25**	**103 ± 6**	**97 ± 11**	**119 ± 3**

Table S1.

Cell viability is unaffected by temperature cycling. A single yeast preculture was grown, diluted to OD_{600} = 0.50 ± 0.03, and then subjected to the protocol in Figure S7*A*. Within experimental uncertainty (which is calculated as standard deviation = S.D.) the average number of colonies in samples 1, 2, and 3 are indistinguishable from the control.

Step	Temp (˚C)	Duration (mm:ss)
1	25	15:00
2	45	0:01
3	35	0:01
4	32.6	0:01
5	31.1	0:01
6	30.4	0:01
7	29	0:01
8	28	2:00
9	27	2:00
10	26	2:00
11	25.4	0:01
12	Go to step 2, twice	

Step	Temp (˚C)	Duration (mm:ss)
13	42.5	0:01
14	41.6	0:19
15	44.1	0:01
16	35.1	0:01
17	34.1	0:01
18	33.1	0:01
19	32.1	0:01
20	31.1	0:01
21	29.6	2:00
22	28.7	2:00
23	28.2	1:42
24	30.4	0:10

Step	Temp (˚C)	Duration (mm:ss)
25	32.6	0:10
26	34.8	0:10
27	36.9	0:01
28	38	0:10
29	39	0:01
30	35	0:01
31	33.9	0:01
32	32.8	0:01
33	32.1	0:01
34	31	0:10
35	29.9	0:30
36	Go to step 24, twice	

Table S2.

Temperature cycling protocol. Within the cell viability assay illustrated in Fig. S7*A*, the temperature of sample 3 in Table S1 was varied in a MJ Mini Thermal Cycler (BIO-RAD, Hercules, CA) using the protocol in this table. Steps 24-36 mimic the conditions of Fig. 8 in the main text and in Fig. S6. The entire protocol elapses over 57 min, 35 seconds. “Duration” denotes the time for which the particular temperature was held once it was reached, before moving to the next programmed temperature.

Figure/Movie	Microscopy Technique	Temperature Conditions	System	Osmotic Gradient
Fig. 6*A*	Standard epifluorescence	25°C	Synthetic GUV membrane	No
Fig. 6*B*	"Control" conditions in reference (29)	10°C	Giant plasma membrane vesicle	No
Fig. 6*C*	Wide-field illumination, iterative deconvolution, and structured illumination	Ambient (~22°C)	*In vivo* yeast vacuole	No
Fig. 7/Movie S1	Iterative deconvolution	Ambient (~22°C)	*In vivo* yeast vacuole	Yes
Fig. 8/Movie S4	HILO illumination	Thermal cycling	*In vivo* yeast vacuole	No
Fig. 9/Movie S6	HILO illumination	Thermal cycling	Cell-free yeast vacuole	No
Fig. S1	Wide-field illumination and differential interference contrast	Ambient (~22°C)	*In vivo* yeast vacuole	No
Fig. S2	Standard illumination (by Joan Bleecker)	Constant temperature	Synthetic GUV membrane	No
Fig. S3*A*/Movie S2	Iterative deconvolution	Ambient (~22°C)	*In vivo* yeast vacuole	Yes
Fig. S3*B*	Wide-field illumination	Ambient (~22°C)	*In vivo* yeast vacuole	Yes
Fig. S4/Movie S3	Iterative deconvolution	Ambient (~22°C)	*In vivo* yeast vacuole	Yes
Fig. S5	N/A – sketch of membrane coexisting phase behavior			
Fig. S6/Movie S5	HILO illumination	Thermal cycling	*In vivo* yeast vacuole	No
Fig. S7*A*, *B*	N/A – sketch of growth protocols			
Fig. S7*C*	N/A – growth curve for yeast strain *MAT α his3Δ1 lys2Δ0 ura3Δ0 leu2Δ0 VPH1-GFP::HIS3MX6*			
Fig. S8	HILO illumination	Thermal cycling	Cell-free yeast vacuole	No
Fig. S9/Movies S7 and S9	HILO illumination	Thermal cycling	*In vivo* yeast vacuole	No
Fig. S10/Movie S8	Standard epifluorescence	Thermal cycling	Synthetic GUV membrane	No

Table S3.

A summary of conditions and methods used with each experiment presented in the figures and movies of the main text and this *SI Appendix*.

Movie S1.
A video of *in vivo* vacuole domains merging and their subsequent rearrangement as shown in Fig. 7. This movie plays at ~10x speed.

Movie S2.
A video of *in vivo* vacuole domains merging and their subsequent rearrangement as shown in Fig. S3*A*. This movie plays at ~30x speed.

Movie S3.
A video of *in vivo* vacuole domains becoming smaller as shown in Fig. S4. The left half corresponds to the top hemisphere of the vacuole and the right half corresponds to the bottom hemisphere. This movie plays at ~30x speed.

Movie S4.
A video of *in vivo* vacuole domains vanishing and reappearing with the temperature cycle shown in Fig. 8 as an inset in a plot of temperature through time. The movie plays at ~3x speed.

Movie S5.
A video of *in vivo* vacuole domains vanishing and reappearing with the temperature cycle shown in Fig. S6 as an inset in a plot of temperature through time. The movie plays at ~3x speed.

Movie S6.
A video of cell-free vacuole domains vanishing and reappearing with the temperature cycle shown in Figs. 9 and S8-bottom. The movie plays at ~3x speed.

Movie S7.
A video of *in vivo* vacuole domains vanishing and reappearing with a rapid heat cycle as shown in Fig. S9-rapid. The movie plays at ~3x speed.

Movie S8.
A video of giant unilamellar vesicle (GUV) domains vanishing and reappearing with fast vs. slow temperature ramps as shown in Fig. S10. The movie plays at ~10x speed.

Movie S9.
A video of *in vivo* vacuole domains vanishing and reappearing with a slow temperature cycle as shown in Fig. S9-slow. The movie plays at ~3x speed.

CHAPTER 5

References

1. Simons, K. & Toomre, D. Lipid rafts and signal transduction. *Nat. Rev. Mol. Cell Biol.* **1,** 31–39 (2000).
2. Lingwood, D. & Simons, K. Lipid Rafts As a Membrane-Organizing Principle. *Science (80-.).* **327,** 46–50 (2010).
3. Munro, S. Lipid Rafts: Elusive or Illusive? *Cell* **115,** 377–388 (2003).
4. Veatch, S. L. & Keller, S. L. Organization in Lipid Membranes Containing Cholesterol. *Phys. Rev. Lett.* **89,** 268101 (2002).
5. Baumgart, T., Hess, S. T. & Webb, W. W. Imaging coexisting fluid domains in biomembrane models coupling curvature and line tension. *Nature* **425,** 821–824 (2003).
6. Honerkamp-Smith, A. R. *et al.* Line Tensions, Correlation Lengths, and Critical Exponents in Lipid Membranes Near Critical Points. *Biophys. J.* **95,** 236–246 (2008).
7. Brangwynne, C. P. Phase transitions and size scaling of membrane-less organelles. *The Journal of cell biology* **203,** 875–881 (2013).
8. Hyman, A. A., Weber, C. A. & Jülicher, F. Liquid-Liquid Phase Separation in Biology. *Annu. Rev. Cell Dev. Biol.* **30,** 39–58 (2014).
9. Angelova, M. I., Soléau, S., Méléard, P., Faucon, F. & Bothorel, P. Preparation of giant vesicles by external AC electric fields. Kinetics and applications. in *Trends in Colloid and Interface Science VI* 127–131 (Steinkopff, 1992). doi:10.1007/BFb0116295
10. Veatch, S. L. & Keller, S. L. Separation of Liquid Phases in Giant Vesicles of Ternary Mixtures of Phospholipids and Cholesterol. *Biophys. J.* **85,** 3074–3083 (2003).
11. Blosser, M. C., Cornell, C. E., Rayermann, S. P. & Keller, S. L. Chapter 18. Phase Diagrams and Tie Lines in GUVs. in *The Giant Vesicle Book* (eds. Dimova, R. & Marques, C.) (Boca Raton: Taylor & Francis / CRC Press).
12. Lingwood, D., Ries, J., Schwille, P. & Simons, K. Plasma membranes are poised for activation of raft phase coalescence at physiological temperature. *Proc. Natl. Acad. Sci. USA* **105,** 10005–10010 (2008).
13. Veatch, S. L. *et al.* Critical fluctuations in plasma membrane vesicles. *ACS Chem. Biol.* **3,** 287–293 (2008).
14. Keller, S. L. *et al.* Probability of alamethicin conductance states varies with nonlamellar tendency of bilayer phospholipids. *Biophys. J.* **65,** 23–27 (1993).
15. Cornea, R. L. & Thomas, D. D. Effects of membrane thickness on the molecular dynamics and enzymatic activity of reconstituted Ca-ATPase. *Biochemistry* **33,** 2912–2920 (1994).
16. Cornelius, F. Modulation of Na,K-ATPase and Na-ATPase activity by phospholipids and cholesterol. I. Steady-state kinetics. *Biochemistry* **40,** 8842–8851 (2001).
17. Kahya, N., Brown, D. & Schwille, P. Raft partitioning and dynamic behavior of human placental alkaline phosphatase in giant unilamellar vesicles. *Biochemistry* **44,** 7479–7489 (2005).
18. Levental, I., Grzybek, M. & Simons, K. Greasing their way: Lipid modifications determine protein association with lipid rafts. *Biochemistry* **49,** 6305–6316 (2010).
19. Lin, Q. & London, E. Altering hydrophobic sequence lengths shows that hydrophobic

mismatch controls affinity for ordered lipid domains (rafts) in the multitransmembrane strand protein perfringolysin O. *J. Biol. Chem.* **288,** 1340–1352 (2013).
20. *The Giant Vesicle Book*. (Boca Raton: Taylor & Francis / CRC Press).
21. Bagatolli, L. A. To see or not to see: Lateral organization of biological membranes and fluorescence microscopy. *BBA-Biomembranes* **1758,** 1541–1556 (2006).
22. Klymchenko, A. S. & Kreder, R. Fluorescent probes for lipid rafts: From model membranes to living cells. *Chem. Biol.* **21,** 97–113 (2014).
23. Sezgin, E., Sadowski, T. & Simons, K. Measuring lipid packing of model and cellular membranes with environment sensitive probes. *Langmuir* **30,** 8160–8166 (2014).
24. Silvius, J. R. Fluorescence energy transfer reveals microdomain formation at physiological temperatures in lipid mixtures modeling the outer leaflet of the plasma membrane. *Biophys. J.* **85,** 1034–1045 (2003).
25. Baumgart, T., Hunt, G., Farkas, E. R., Webb, W. W. & Feigenson, G. W. Fluorescence probe partitioning between Lo/Ld phases in lipid membranes. *Biochim. Biophys. Acta* **1768,** 2182–2194 (2007).
26. Sezgin, E. *et al.* Partitioning, diffusion, and ligand binding of raft lipid analogs in model and cellular plasma membranes. *Biochim. Biophys. Acta* **1818,** 1777–1784 (2012).
27. Veatch, S. L. & Keller, S. L. Separation of liquid phases in giant vesicles of ternary mixtures of phospholipids and cholesterol. *Biophys. J.* **85,** 3074–3083 (2003).
28. Juhasz, J., Sharom, F. J. & Davis, J. H. Quantitative characterization of coexisting phases in DOPC/DPPC/cholesterol mixtures: Comparing confocal fluorescence microscopy and deuterium nuclear magnetic resonance. *BBA-Biomembranes* **1788,** 2541–2552 (2009).
29. Stanich, C. A. *et al.* Coarsening dynamics of domains in lipid membranes. *Biophys. J.* **105,** 444–454 (2013).
30. Dietrich, C. *et al.* Lipid rafts reconstituted in model membranes. *Biophys. J.* **80,** 1417–1428 (2001).
31. Samsonov, A. V, Mihalyov, I. & Cohen, F. S. Characterization of cholesterol-sphingomyelin domains and their dynamics in bilayer membranes. *Biophys. J.* **81,** 1486–1500 (2001).
32. Rozovsky, S., Kaizuka, Y. & Groves, J. T. Formation and spatio-temporal evolution of periodic structures in lipid bilayers. *J. Amer. Chem. Soc.* **127,** 36–37 (2005).
33. Yanagisawa, M., Imai, M., Masui, T., Komura, S. & Ohta, T. Growth dynamics of domains in ternary fluid vesicles. *Biophys. J.* **92,** 115–125 (2007).
34. Semrau, S. & Schmidt, T. Membrane heterogeneity - from lipid domains to curvature effects. *Soft Matter* **5,** 3129–3364 (2009).
35. Ursell, T. S., Klug, W. S. & Phillips, R. Morphology and interaction between lipid domains. *Proc. Natl. Acad. Sci. USA* **106,** 13301–13306 (2009).
36. Hu, J., Weikl, T. R. & Lipowsky, R. Vesicles with multiple membrane domains. *Soft Matter* **7,** 6092 (2011).
37. Honerkamp-Smith, A. R., Veatch, S. L. & Keller, S. L. An introduction to critical points for biophysicists: Observations of compositional heterogeneity in lipid membranes. *Biochim. Biophys. Acta* **1788,** 53–63 (2009).
38. Veatch, S. L., Soubias, O., Keller, S. L. & Gawrisch, K. Critical fluctuations in domain-forming lipid mixtures. *Proc. Natl. Acad. Sci. USA* **104,** 17650–17655 (2007).
39. Honerkamp-Smith, A. R., Veatch, S. L. & Keller, S. L. Line tensions, correlation lengths, and critical exponents in lipid membranes near critical points. *Biophys. J.* **95,** 236–246

(2008).
40. Inaura, K. & Fujitani, Y. Concentration fluctuation in a two-component fluid membrane surrounded with three-dimensional fluids. *J. Phys. Soc. Jpn.* **77,** 114603 (2008).
41. Haataja, M. Critical dynamics in multicomponent lipid membranes. *Phys. Rev. E* **80,** 20902 (2009).
42. Honerkamp-Smith, A. R., Machta, B. B. & Keller, S. L. Experimental observations of dynamic critical phenomena in a lipid membrane. *Phys. Rev. Lett.* **108,** 1–5 (2012).
43. Connell, S. D., Heath, G., Olmsted, P. D. & Kisil, A. Critical point fluctuations in supported lipid membranes. *Faraday Discuss.* **161,** 91–111 (2013).
44. Davis, J. H., Ziani, L. & Schmidt, M. L. Critical fluctuations in DOPC/DPPC-d62/cholesterol mixtures: 2H magnetic resonance and relaxation. *J. Chem. Phys.* **139,** 45104 (2013).
45. Esposito, C. *et al.* Ficker spectroscopy of thermal lipid bilayer domain boundary fluctuations. *Biophys. J.* **93,** 3169–3181 (2007).
46. Tian, A., Johnson, C., Wang, W. & Baumgart, T. Line tension at fluid membrane domain boundaries measured by micropipette aspiration. *Phys. Rev. Lett.* **98,** 208102 (2007).
47. Veatch, S. L. *et al.* Critical Fluctuations in Plasma Membrane Vesicles. *ACS Chem. Biol.* **3,** 287–293 (2008).
48. Levental, I., Grzybek, M. & Simons, K. Raft domains of variable properties and compositions in plasma membrane vesicles. *Proc. Natl. Acad. Sci. USA* **108,** 11411–11416 (2011).
49. Sezgin, E. *et al.* Elucidating membrane structure and protein behavior using giant plasma membrane vesicles. *Nat. Protoc.* **7,** 1042–1051 (2012).
50. Furuya, K. & Mitsui, T. Phase transitions in bilayer membranes of dioleoyl-phosphatidylcholine/dipalmitoyl-phosphatidylcholine. *J. Phys. Soc. Jpn.* **46,** 611–616 (1979).
51. Korlach, J., Schwille, P., Webb, W. W. & Feigenson, G. W. Characterization of lipid bilayer phases by confocal microscopy and fluorescence correlation spectroscopy. *Proc. Natl. Acad. Sci. USA* **96,** 8461–8466 (1999).
52. Bagatolli, L. A. & Gratton, E. A correlation between lipid domain shape and binary phospholipid mixture composition in free standing bilayers: A two-photon fluorescence microscopy study. *Biophys. J.* **79,** 434–447 (2000).
53. Feigenson, G. W. & Buboltz, J. T. Ternary phase diagram of dipalmitoyl-PC/Dilauroyl-PC/cholesterol: Nanoscopic domain formation driven by cholesterol. *Biophys. J.* **80,** 2755–2788 (2001).
54. Zhao, J. *et al.* Phase studies of model biomembranes: Macroscopic coexistence of La+Lb, with light-induced coexistence of La+Lo phases. *Biochim. Biophys. Acta* **1768,** 2777–2786 (2007).
55. Fidorra, M., Duelund, L., Leidy, C., Simonsen, A. C. & Bagatolli, L. A. Absence of fluid-ordered/fluid-disordered phase coexistence in ceramide/POPC mixtures containing cholesterol. *Biophys. J.* **90,** 4437–4451 (2006).
56. Margineanu, A. *et al.* Visualization of membrane rafts using a perylene monoimide derivative and fluorescence lifetime imaging. *Biophys. J.* **93,** 2877–2891 (2007).
57. Haluska, C. K. *et al.* Combining fluorescence lifetime and polarization microscopy to discriminate phase separated domains in giant unilamellar vesicles. *Biophys. J.* **95,** 5737–5747 (2008).

58. Davis, J. H., Clair, J. J. & Juhasz, J. Phase equilibria in DOPC/DPPC-d62/cholesterol mixtures. *Biophys. J.* **96,** 521–539 (2009).
59. Ionova, I. V, Livshits, V. A. & Marsh, D. Phase diagram of ternary cholesterol/palmitoylsphingomyelin/palmitoyloleoyl-phosphatidylcholine mixtures: Spin-label EPR study of lipid-raft formation. *Biophys. J.* **102,** 1856–1865 (2012).
60. Veatch, S. L. & Keller, S. L. Seeing spots: Complex phase behavior in simple membranes. *Biochim. Biophys. Acta* **1746,** 172–185 (2005).
61. Goñi, F. M. *et al.* Phase diagrams of lipid mixtures relevant to the study of membrane rafts. *Biochim. Biophys. Acta* **1781,** 665–684 (2008).
62. Morales-Penningston, N. F. *et al.* GUV preparation and imaging: Minimizing artifacts. *Biochim. Biophys. Acta* **1798,** 1324–1332 (2010).
63. Bezlyepkina, N., Gracia, R. S., Shchelokovskyy, P., Lipowsky, R. & Dimova, R. Phase diagram and tie-line determination for the ternary mixture DOPC/eSM/cholesterol. *Biophys. J.* **104,** 1456–1464 (2013).
64. Levental, I. *et al.* Cholesterol-dependent phase separation in cell-derived membrane vesicles. *Biochem. J.* **424,** 163–167 (2009).
65. Gray, E., Karslake, J., Machta, B. B. & Veatch, S. L. Liquid general anesthetics lower critical temperatures in plasma membrane vesicles. *Biophys. J.* **105,** 2751–2759 (2013).
66. Machta, B. B. *et al.* Conditions that stabilize membrane domains also antagonize n-alcohol anesthesia. *Biophys. J.* **111,** 537–545 (2016).
67. Veatch, S. L., Leung, S. S. W., Hancock, R. E. W. & Thewalt, J. L. Fluorescent probes alter miscibility phase boundaries in ternary vesicles. *J. Phys. Chem B* **111,** 502–504 (2007).
68. Kaiser, H.-J. *et al.* Order of lipid phases in model and plasma membranes. *Proc. Natl. Acad. Sci. USA* **106,** 16645–16650 (2009).
69. Kim, H. M. *et al.* A two-photon fluorescent probe for lipid raft imaging: C-Laurdan. *ChemBioChem* **8,** 553–559 (2007).
70. Sezgin, E., Waithe, D., Bernadino de la Serna, J. & Eggeling, C. Spectral imaging to measure heterogeneity in membrane lipid packing. *ChemPhysChem* **16,** 1387–1394 (2015).
71. Portet, T., Gordon, S. E. & Keller, S. L. Increasing membrane tension decreases miscibility temperatures; an experimental demonstration via micropipette aspiration. *Biophys. J.* **103,** L35–L37 (2012).
72. Uline, M. J., Schick, M. & Szleifer, I. Phase behavior of lipid bilayers under tension. *Biophys. J.* **102,** 517–522 (2012).
73. Oglecka, K., Rangamani, P., Liedberg, B., Kraut, R. S. & Parikh, A. N. Oscillatory phase separation in giant lipid vesicles induced by transmembrane osmotic differentials. *Elife* **3,** e03695 (2014).
74. Ayuyan, A. G. & Cohen, F. S. Lipid peroxides promote large rafts: Effects of excitation of probes in fluorescence microscopy and electrochemical reactions during vesicle formation. *Biophys. J.* **91,** 2172–2183 (2006).
75. Roux, A. *et al.* Role of curvature and phase transition in lipid sorting and fission of membrane tubules. *EMBO J.* **24,** 1537–1545 (2005).
76. Loftus, A. F., Noreng, S., Hsieh, V. L. & Parthasarathy, R. Robust measurement of membrane bending moduli using light sheet fluorescence imaging of vesicle fluctuations. *Langmuir* **29,** 14588–14594 (2013).

77. Blosser, M. C., Honerkamp-Smith, A. R., Han, T., Haataja, M. & Keller, S. L. Transbilayer colocalization of liquid domains explained via measurement of strong coupling parameters. *Biophys. J.* **109,** 2317–2327 (2015).
78. Yang, J. & Appleyard, J. The main phase transition of mica-supported phosphatidylcholine membranes. *J. Phys. Chem B* **104,** 8097–8100 (2000).
79. Yarrow, F., Vlugt, T. J. H., van der Eerden, J. P. J. M. & Snel, M. M. E. Melting of a DPPC lipid bilayer observed with atomic force microscopy and computer simulation. *J. Cryst. Growth* **275,** e1417–e1421 (2005).
80. Gordon, V. D., Deserno, M., Andrew, C. M. J., Egelhaaf, S. U. & Poon, W. C. K. Adhesion promotes phase separation in mixed-lipid membranes. *Eur. Lett.* **84,** 48003 (2008).
81. Zhao, J., Wu, J. & Veatch, S. L. Adhesion stabilizes robust heterogeneity in supercritical membranes at physiological temperature. *Biophys. J.* **104,** 825–834 (2013).
82. Johnson, S. A. *et al.* Temperature-dependent phase behavior and protein partitioning in giant plasma membrane vesicles. (2010). doi:10.1016/j.bbamem.2010.03.009
83. Levental, I., Grzybek, M., Simons, K. & Klein, M. L. Raft domains of variable properties and compositions in plasma membrane vesicles. doi:10.1073/pnas.1105996108
84. Gray, E. M., Díaz-Vázquez, G. & Veatch, S. L. Growth conditions and cell cycle phase modulate phase transition temperatures in RBL-2H3 derived plasma membrane vesicles. *PLoS One* **10,** (2015).
85. Sezgin, E. *et al.* Elucidating membrane structure and protein behavior using giant plasma membrane vesicles. *Nat. Protoc.* **7,** 1042–1051 (2012).
86. Moor, H. & Mühlethaler, K. Fine Structure in Frozen-Etched Yeast Cells. *J. Cell Biol.* **17,** 609–28 (1963).
87. Matile, P., Moor, H. & Robinow, C. F. Chapter 6: Yeast Cytology. in *The Yeasts* (eds. Rose, A. H. & Harrison, J. S.) 219–302 (Academic Press, 1969).
88. Toulmay, A. & Prinz, W. A. Direct imaging reveals stable, micrometer-scale lipid domains that segregate proteins in live cells. *J. Cell Biol.* **202,** 35–44 (2013).
89. Wang, C. W., Miao, Y. H. & Chang, Y. S. A sterol-enriched vacuolar microdomain mediates stationary phase lipophagy in budding yeast. *J. Cell Biol.* **206,** 357–366 (2014).
90. Tsuji, T. *et al.* Niemann-Pick type C proteins promote microautophagy by expanding raft-like membrane domains in the yeast vacuole. (2017). doi:10.7554/eLife.25960.001
91. Moeller, C. H., Mudd, J. B. & Thomson, W. W. LIPID PHASE SEPARATIONS AND INTRAMEMBRANOUS PARTICLE MOVEMENTS IN THE YEAST TONOPLAST. **643,** 376–386 (1981).
92. Samsonov, A. V, Mihalyov, I. & Cohen, F. S. Characterization of Cholesterol-Sphingomyelin Domains and Their Dynamics in Bilayer Membranes.
93. Stanich, C. A. *et al.* Coarsening dynamics of domains in lipid membranes. *Biophys. J.* **105,** 444–454 (2013).
94. Moeller, C. H. & Thomson, W. W. An Ultrastructural Study of the Yeast Tonoplast during the Shift from Exponential to Stationary Phase. *J. Ultrastruct. Res.* **68,** 28–37 (1979).
95. *The Yeasts*. (Academic Press, 1969).
96. Goffeau, A. *et al.* Life with 6000 genes. *Science* **274,** 546, 563–7 (1996).
97. Botstein, D. & Fink, G. R. Yeast: An Experimental Organism for 21st Century Biology. doi:10.1534/genetics.111.130765
98. Baker Brachmann, C. *et al.* Designer deletion strains derived fromSaccharomyces

cerevisiae S288C: A useful set of strains and plasmids for PCR-mediated gene disruption and other applications. *Yeast* **14,** 115–132 (1998).
99. Steinmetz, L. M. *et al.* Systematic screen for human disease genes in yeast. *Nat Genet* **31,** 400–404 (2002).
100. Haber, J. E. Mating-Type Genes and MAT Switching in Saccharomyces cerevisiae. *Yeastbook* **191,** 33–64 (2012).
101. Fowell, R. R. Chapter 7: Sporulation and Hybridization of Yeasts. in *The Yeasts* (eds. Rose, A. H. & Harrison, J. S.) 303–383 (Academic Press, 1969).
102. Martin, S. G., Merlini, L. & Dudin, O. Mate and fuse: how yeast cells do it. *Open Biol.* **3,** 130008 (2013).
103. Tokunaga, M., Imamoto, N. & Sakata-Sogawa, K. Highly inclined thin illumination enables clear single-molecule imaging in cells. *Nat. Methods* **5,** 159–161 (2008).
104. Konopka, C. A. & Bednarek, S. Y. Variable-angle epifluorescence microscopy: A new way to look at protein dynamics in the plant cell cortex. *Plant J.* **53,** 186–196 (2008).
105. Robinow, C. F. & Marak, J. A FIBER APPARATUS IN THE NUCLEUS OF THE YEAST CELL. *J. Cell Biol.* **29,** 129–151 (1966).
106. Jones, H. D., Schliwa, M. & Drubin, D. G. Video microscopy of organelle inheritance and motility in budding yeast. *Cell Motil. Cytoskeleton* **25,** 129–142 (1993).
107. Veatch, S. L. & Keller, S. L. Organization in lipid membranes containing cholesterol. *Phys. Rev. Lett.* **89,** 1–4 (2002).
108. Schneiter, R. *et al.* Analysis of the Lipid Molecular Species Composition of Yeast Subcellular Membranes Reveals Acyl Chain-based Sorting / Remodeling of Distinct Molecular Species En Route to the Plasma Membrane. *J. Cell Biol.* **146,** 741–754 (1999).
109. Zinser, E. *et al.* Phospholipid synthesis and lipid composition of subcellular membranes in the unicellular eukaryote Saccharomyces cerevisiae. *J. Bacteriol.* **173,** 2026–2034 (1991).
110. Beattie, M. E., Veatch, S. L., Stottrup, B. L. & Keller, S. L. Sterol Structure Determines Miscibility versus Melting Transitions in Lipid Vesicles. *Biophys. J.* **89,** 1760–1768 (2005).
111. Moeller, C. H. & Thomson, W. W. Uptake of lipid bodies by the yeast vacuole involving areas of the tonoplast depleted of intramembranous particles. *J. Ultrasructure Res.* **68,** 38–45 (1979).
112. Chozinski, T. J. *et al.* Expansion microscopy with conventional antibodies and fluorescent proteins. *Nat. Methods* **13,** 485–488 (2016).
113. Lira, R. B., Steinkühler, J., Knorr, R. L., Dimova, R. & Riske, K. A. Posing for a picture: vesicle immobilization in agarose gel. *Sci. Rep.* **6,** 25254 (2016).
114. Bacia, K., Schwille, P. & Kurzchalia, T. Sterol structure determines the separation of phases and the curvature of the liquid-ordered phase in model membranes. *Proc. Natl. Acad. Sci.* **102,** 3272–3277 (2005).
115. Hamada, T. *et al.* Dynamic processes in endocytic transformation of a raft-exhibiting giant liposome. *J. Phys. Chem. B.* **111,** 10853–10857 (2007).
116. Wintersmith, J. R. *et al.* Determination of interphase line tension in Langmuir films. *Phys. Rev. E - Stat. Nonlinear, Soft Matter Phys.* **75,** 61605 (2007).
117. Williams, S. P., Haggie, P. M. & Brindle, K. M. 19F NMR measurements of the rotational mobility of proteins in vivo. *Biophys. J.* **72,** 490–498 (1997).
118. Fujino, T., Hirota, K., Ohta, K. & Tahara, T. In-cell Viscosity Measurement Using a Fluorescence Up-conversion Microscope. *Chem. Lett.* **37,** 1240–1241 (2008).

119. Nicolini, C. *et al.* Temperature and pressure effects on structural and conformational properties of POPC/SM/cholesterol model raft mixtures-a FT-IR, SAXS, DSC, PPC and Laurdan fluorescence spectroscopy study. *Biochim. Biophys. Acta - Biomembr.* **1758,** 248–258 (2006).
120. Bagnat, M. & Simons, K. Cell surface polarization during yeast mating. *Proc. Natl. Acad. Sci.* **99,** 14183–14188 (2002).
121. Wedlich-Soldner, R., Altschuler, S., Wu, L. & Li, R. Spontaneous cell polarization through actomyosin-based delivery of the Cdc42 GTPase. *Science (80-.).* **299,** 1231–1235 (2003).
122. Makushok, T. *et al.* Sterol-Rich Membrane Domains Define Fission Yeast Cell Polarity. *Cell* **165,** 1182–1196 (2016).
123. Takatori, S. *et al.* Phosphatidylinositol 3,5-Bisphosphate-Rich Membrane Domains in Endosomes and Lysosomes. *Traffic* **17,** 154–167 (2016).
124. Wang, L., Seeley, E. S., Wickner, W. & Merz, A. J. Vacuole Fusion at a Ring of Vertex Docking Sites Leaves Membrane Fragments within the Organelle. *Cell* **108,** 357–369 (2002).
125. Fratti, R. A., Jun, Y., Merz, A. J., Margolis, N. & Wickner, W. Interdependent assembly of specific regulatory lipids and membrane fusion proteins into the vertex ring domain of docked vacuoles. *J. Cell Biol.* **167,** 1087–1098 (2004).
126. McNally, E. K., Karim, M. A. & Brett, C. L. Selective Lysosomal Transporter Degradation by Organelle Membrane Fusion. *Dev. Cell* **40,** 151–167 (2017).
127. Lockshon, D. *et al.* Rho Signaling Participates in Membrane Fluidity Homeostasis. *PLoS One* **7,** (2012).

Appendix: Yeast Lysis and Vacuole Isolation Protocol

This section is taken from a cell lysis and vacuole isolation protocol optimized by the Merz lab

Cell Lysis Procedure

This section is modified from a protocol written up by Liz Manroe

1. Grow up culture: 43 Hours ahead of when you want cells with many half-moon vacuoles, start 3 colonies of yeast strain AMY 1089 (BY 4742 background) in 200 ml of Synthetic complete media.

2. Harvest culture at OD_{600} = 6.8-7.8.
   - Calculate the volume of culture to use by employing the following equation:
     $$x = \frac{1000\ ml * OD_{600}}{y},$$
     where y is the OD_{600} value of the culture (and has units of OD_{600}) and x is the volume to be used for the rest of the procedure
   - Transfer x ml into an appropriately sized centrifuge tube
     In order to minimize sloshing, which can imbalance a centrifuge, you want any given centrifuge tube being used to be as close to full capacity as possible
   - ***Centrifuge at 4000 rpm for 10 minutes at room temperature***
     I will denote this in the future as: ***[4000 rpm, 10 minutes, 25 °C]***
   - During spin:
     - Turn on water bath to 30 °C
     - Make **wash buffer**
   - After the spin, save ~10 ml of the supernatant (depleted media) for each x ml pellet; discard the rest of the supernatant

3. Wash the cells by re-suspending each x ml pellet in 50 ml of **wash buffer**
   - Transfer each suspension into a 50 ml disposable, plastic centrifuge tube
   - ***Incubate in 30 °C water bath for 10 minutes***, swirling occasionally.
   - During incubation:
     - Chill SW-41 tubes on ice
     - Thaw oxalyticase if frozen, move to ice if stored in cold room
     - Make **spheroplasting buffer**
       - Spin down the depleted media again at 14000 rpm, 1 min before use
   - ***Centrifuge [4000 rpm, 5 minutes, 25 °C]***
   - Save the pellet, discard supernatant

4. Spheroplast with oxalyticase
   - Re-suspend pellet in **spheroplasting buffer** (15 ml per pellet)
   - Swirl by hand (with rests on ice) until re-suspended

- ***Add oxalyticase*** (2 ml per pellet)
- ***Shake vigorously 2-4 times*** to mix
- ***Incubate at 30 °C for 1 hour***, gently rotating the tube from perpendicular to parallel with the floor 1-2 times to "swirl" a few times during the incubation
- During incubation:
    - Prepare **DEAE-Dextran solution**
    - Start ultracentrifuge (make sure it begins cooling to 4 °C)
    - Begin cooling a swinging bucket centrifuge down to 4 °C

5. Treat with DEAE-dextran
- ***Centrifuge [4000 rpm, 5 minutes, 4 °C]***
- Remove to ice, supernatant should be just slightly cloudy
- Remove and discard supernatant using vacuum. Pellet should be gelatinous, not rigid
- ***Add 2.0 ml of 15% ficoll to each pellet*** and re-suspend with vigorous swirling
  Takes ~ 0.5 hrs. Swirl by holding the tube parallel to the floor and moving your hand side-to-side. Pellet will begin to separate after 5-10 min and will look very stringy. Target clump size is ~5mm or smaller.
- ***Add* DEAE-dextran solution** (20 µl)
- ***Incubate 2 minutes on ice, then 3 minutes at 30 °C*** with occasional swirling
- ***Remove immediately to ice***

One can image directly at this point, using Differential Interference Microscopy to confirm any given vacuole is outside its cell. To fully isolate the vacuoles:

6. Prepare flotation gradient in pre-chilled SW-40 or 41 tubes.
- Load 3-4 ml of yeast lysate at bottom of tube. Use suction to remove any bubbles
  Use a 1 ml digital pipet whose tip has been cut so the opening is ~5 mm in diameter. Draw up into the pipet and deposit from the pipet as slowly as possible. These minimize sheer forces on the vacuoles.
- Overlay with 3 ml of 8%, then 3 ml of 4% ficoll
  Use a 3 ml syringe, deposit solutions at a rate of ~12.5 µL/second (~4 minutes to deposit 3 ml)
- Fill to within 5 mm of the top with PS buffer ("0% ficoll")

7. Ultracentrifuge in SW-40 or -41 rotor at **[30,000 (30K) rpm, 90 minutes, 4 °C]**

8. Harvest vacuoles
- Trim the tip of a 200 µl pipet tip to make a ~5 mm opening and place on a digital pipet set to 200 µl
- Target the white material sitting at the interface of the 4% ficoll and PS buffer
- Depress the pipet to the first stop, insert the tip into the 4% ficoll/PS buffer interface, and use the pipet tip to swirl from the outer edge inwards, with a slight upwards motion. This will gather the white material together and move it more into the PS buffer (we want our vacuoles in PS buffer)
- Aim the tip at this accumulated mass and as slowly as possible, pull 200 µl into the pipet
- Repeat this process, removing the vacuole suspension in 200 µl batches, storing each batch on wet ice until used

Fusion assay work indicates vacuoles are useable for 3 hours after ultracentrifugation

Day-of Reagent Preparation (to be made during procedure)

Note: because a centrifuge must be balanced to avoid damage, the following solutions are designed to make sufficient volumes for two samples to be run in parallel. If only doing one run, you can cut the amounts in half and make sure you use water or some such to create a counterbalance during all centrifugation steps.

Wash buffer

90 ml of deionized water
10 ml of 1 M Tris-HCl pH 9.4
0.154 g of Dithiothreitol (DTT)
Make 50 ml per sample

Spheroplasting buffer

2 ml of 1 M potassium phosphate (KP_i) pH 7.5
3.2 ml of depleted media*
6 ml of 4 M sorbitol
28.8 ml of deionized water
Make 20 ml per sample
*As aforementioned, this is taken from the supernatant of the first centrifugation step

DEAE-Dextran

Float 10 mg DEAE-Dextran
on 1 ml of 15% ficoll
After a few minutes, vortex into solution
Store on ice

Stock Reagent Preparation (to be done before starting the procedure)

1 M Tris-HCl pH 9.4 500 ml

60.5 g Tris-Base ICN819638
Add 400 ml deionized water
Adjust pH to 9.4 with 10 M HCl
Bring to 500 ml with deionized water
Store at room temperature

1 M Pipes-KOH pH 6.8 500 ml
151 grams Pipes Sigma P6757
Add 300 ml deionized water
Adjust pH to 6.8 with 10 M KOH

Note: Add a couple of ml at a time and then dropwise to finish. The solution will appear milky until the pH is close to 6.8

Bring to 50 ml with deionized water
Store long-term at -20 °C freezer
Store up to 2 weeks at 4 °C
Suggested aliquot size: 20 ml

4 M Sorbitol 500 ml

364 g Sorbitol Sigma S1876
Add 200 ml deionized water and mix with a stir rod until it is a paste. Heating in a microwave will facilitate this process. Use magnetic stirrer until the solution is clear.
Adjust the volume to 500 ml with additional deionized water.
Store at room temperature.

PS Buffer (a.k.a. 0% ficoll) 1 liter

Add 1 M Pipes pH 6.8 to 20 mM final concentration 20 ml
Add 4 M Sorbitol to 200 mM final concentration 50 ml
Bring to 1 liter with deionized water
Store at 4 °C

15% Ficoll 300 ml

45 grams Pharmacia 17-0400-02
200 ml deionized water
Mix with a stir rod until it is a paste and then use a magnetic stirrer to get a clear solution.
Add 1 M Pipes-KOH pH 6.8 to 10 mM final concentration 3 ml
Add 4 M Sorbitol to 200 mM final concentration 15 ml
Bring to 300 ml final volume with deionized water.
Store at 4 °C

8% Ficoll

Prepare from 0% and 15% ficoll

0% Ficoll	15% Ficoll	Total Volume
18.4	21	39.4
36.8	42	78.8
73.6	84	157

Store at 4 °C

4% Ficoll

Prepare by mixing equal volumes of 8% and 0% ficoll.
Store at 4 °C

1 M Potassium Phosphate pH 7.5 100 ml

1 M K_2HPO_4 17.4 g / 100 ml deionized water ~80.0 ml
1 M KH_2PO_4 13.6 g / 100 ml deionized water ~19.8 ml
Mix to pH 7.5
Store at 4 °C